

## N O T I C E

THIS DOCUMENT HAS BEEN REPRODUCED FROM  
MICROFICHE. ALTHOUGH IT IS RECOGNIZED THAT  
CERTAIN PORTIONS ARE ILLEGIBLE, IT IS BEING RELEASED  
IN THE INTEREST OF MAKING AVAILABLE AS MUCH  
INFORMATION AS POSSIBLE

9950-295

# FORECAST ANALYSIS OF OPTICAL WAVEGUIDE BUS PERFORMANCE

R. LeDesma

Hughes Microelectronic Systems Division  
2601 Campus Drive  
Irvine, CA 92714

M.D. Rourke

Hughes Research Laboratories  
3011 Malibu Canyon Road  
Malibu, CA 90265

October 1979

JPL 955200

Final Report

Period Covered 1 May 1979 through 5 October 1979

(NASA-CR-162851) FORECAST ANALYSIS OF  
OPTICAL WAVEGUIDE BUS PERFORMANCE Final  
Report, 1 May - 5 Oct. 1979 (Hughes Aircraft  
Co., Irvine, Calif.) 76 p HC A09/MF A01

N80-19942

Unclas  
47478

CSSL 20F G3/74

Prepared for  
JET PROPULSION LABORATORIES  
Pasadena, CA



FORECAST ANALYSIS OF OPTICAL WAVEGUIDE  
BUS PERFORMANCE

R. LeDesma  
Hughes Microelectronic Systems Div.  
2601 Campus Drive  
Irvine, CA

M.D. Rourke  
Hughes Research Laboratories  
3011 Malibu Canyon Road  
Malibu, CA 90265

October 1979

JPL 955200

Final Report

Period Covered: 1 May 1979 - 5 October 1979

Prepared for

Jet Propulsion Laboratories  
Pasadena, California

TABLE OF CONTENTS

Section		Page
1	INTRODUCTION . . . . .	7
2	A COMPARISON BETWEEN OPTICAL WAVEGUIDE AND COPPER DATA BUSES . . . . .	9
3	THE ADVANTAGES AND LIMITATIONS OF AN OPTICAL WAVEGUIDE DATA BUS . . . . .	13
4	TEE AND STAR COUPLERS . . . . .	21
	A. Star Couplers . . . . .	21
	B. Tee Couplers . . . . .	29
5	A 32-PORT TRANSMISSIVE STAR COUPLER SYSTEM FOR SPACECRAFT APPLICATION . . . . .	37
	A. Optical Power Budget . . . . .	43
	B. Electrical Power Consumption . . . . .	49
	C. The Effects of Temperature on Bus Performance . . . . .	52
	D. Conclusions . . . . .	62
	REFERENCES . . . . .	65
	APPENDIX I: BIBLIOGRAPHY . . . . .	67
	APPENDIX II: BUS RECEIVER TEST RESULTS . . . . .	69

PRECEDING PAGE BLANK NOT FILMED

LIST OF ILLUSTRATIONS

Figure		Page
1	Attenuation of coaxial and optical waveguide cable as a function of frequency . . . . .	10
2	Optical waveguide attenuation has been dramatically reduced over the past twenty years . . . . .	14
3	Dispersion in optical waveguides has been reduced by more than two orders of magnitude using graded-index multimode and single-mode fibers . . . . .	15
4	A serial data bus employing N access or Tee couplers . . . . .	16
5	A parallel data bus employing a single N-port star coupler . . . . .	16
6	Typical distribution system loss plotted as a function of the number of terminals . . . . .	18
7	A schematic of a fused fiber star coupler including the definitions of various coupler . . . . .	22
8	Configuration of the fused fiber coupler . . . . .	23
9	A bulk optical reflection star coupler . . . . .	27
10	Packing fraction loss is due to the area mismatch between the fiber cores and the area of the mixing rod . . . . .	27
11	The transmission star has fibers attached at each end of the mixing rod . . . . .	28
12	A planar star coupler . . . . .	30
13	The generalized four port optical Tee coupler . . . . .	31
14	Excess loss plotted as a function of tap ratio for 36 fused Tee couplers . . . . .	33
15	A concept for production of planar optical Tee couplers . . . . .	34

**PRECEDING PAGE BLANK NOT FILMED**

Figure		Page
16	Three planar Y couplers are combined to form a planar Tee coupler . . . . .	35
17	A basic 32-port star data bus . . . . .	37
18	An equivalent circuit of a general photodetector and its load resistor $R_L$ . . . . .	38
19	Probability of error from Eq. 25 . . . . .	42
20	A second system configuration employing a reflection star coupler . . . . .	51
21	Temperature dependence of the output power of an LED . . . . .	54
22	Induced attenuation coefficients as a function of temperature for CVD step-index fiber with polyurethane jacket . . . . .	54
23	Amplifier noise model . . . . .	56
24	The expected electrical power consumption of a spacecraft data bus as a function of the number of terminals . . . . .	64

## SECTION 1

### INTRODUCTION

The decision to implement a data bus that incorporates an optical waveguide instead of copper cable will typically depend on many factors. The weight placed on any factor or set of factors will dictate the approach selected. In some bus applications, system cost will be the overriding consideration, while in others it may be to maximize the number of terminals regardless of cost or other factors. In general, the elements to be considered in the design of a data bus include:

- Architecture
- Data rate
- Modulation, encoding, detection
- Power distribution requirements
- Protocol, word structure
- Bus reliability, maintainability
- Interterminal transmission medium
- Cost
- Others specific to application.

This report provides an overview of fiber-optic data bus considerations, specifically addressing a 32-port transmissive star architecture. The format selected is tutorial, with the initial three sections providing a general exposure to optical-waveguide bus concepts. The fourth section addresses the electrical and optical performance of a 32-port transmissive star bus. The last section is an introduction to the effects of temperature on the performance of optical-waveguide buses. Appendix I provides a bibliography of pertinent references. Appendix II provides the bus receiver test results.

## SECTION 2

### A COMPARISON BETWEEN OPTICAL-WAVEGUIDE AND COPPER DATA BUSES

To compare the relative merits of copper cable and optical-waveguide cable, consider first the information carrying capacity  $C$ . For an ideal single channel, the maximum bit rate for a given signal-to-noise ratio ( $S/N$ ) is given by Shannon's relation.

$$C = B \log_2(1 + S/N) \quad , \quad (1)$$

where  $B$  is the channel bandwidth. Maximizing  $B$  and  $S/N$  maximizes the information transfer rate. Unfortunately, the physical properties of transmission lines cause signals to attenuate more rapidly as the signaling frequency increases. However, optical waveguides substantially extend the useful length of a transmission line for any given data rate, as shown in Figure 1. The figure shows typical performance of twisted-shielded-pair, coaxial cable and premium graded-index optical waveguide (4 dB/km, 600 MHz-km range-bandwidth product).

The features of optical waveguide, coaxial cables, and twisted wire pairs are further compared in Table 1. Optical-waveguide cables are superior in terms of signal power loss, weight per unit length, and crosstalk isolation. Coaxial cable is currently superior to the other two media in cost although the price of optical waveguide is rapidly approaching that of coaxial cable.

Another factor that may be considered in system applications is the inherent immunity to electromagnetic pulse (EMP) effects offered by fiber-optic cables. Here again, fiber optics provides a definite advantage over metallic cables. Available data indicate that a great penalty is paid in fabricating coaxial cables to meet stringent EMP protection requirements. For example, a 4-conductor coaxial cable was recently provided by Anaconda. The cable weighs 13,430 pounds per 1000 ft, has an outside diameter of 2.14 in., and costs \$15.00 per meter. Clearly, the added cost and weight of such a cable must be traded off against the degree of EMP immunity desired in the system.

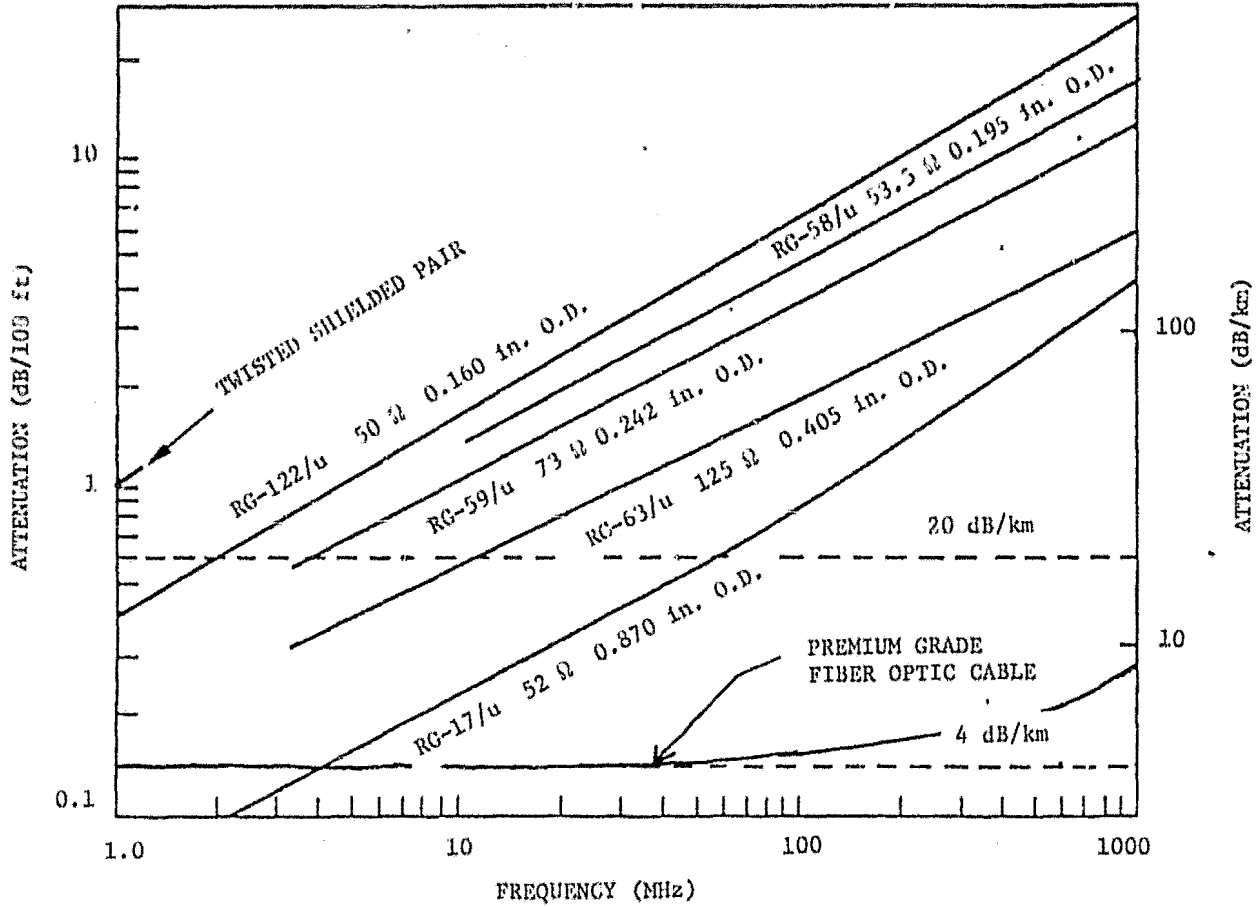


Figure 1. Attenuation of coaxial and optical-waveguide cable as a function of frequency.

Table 1. A Comparison of Transmission Technology

Features	Optical Waveguide	Coaxial Cable	Twisted Wire Pair
Loss of signal power	Low-loss fiber cable, 6 dB/km (Corning #1159 Corguide), 3 dB/km at 400 MHz-km BW	RG-59/U 10 dB/km at 1 MHz BW, 30 dB/km at 10 MHz BW RG-11/U 8 dB/km at 1 MHz BW, 21 dB/km at 10 MHz BW	22 gauge wire pair, 15 dB/km at 1 MHz; Increases exponentially with frequency thereafter
Spacing of repeaters	Typically 8 km	Typically 1.6 to 2.2 km	Not applicable
Bandwidth	400 MHz-km (Corning #1159 Corguide); 1.5 GHz-km (Phillips graded index fiber)	Typically 300 MHz (limited by passband of cable amplifiers)	Approx. 2 to 4 MHz (limited to relatively short distances)
Physical characteristics	Corning Corguide; 17 lb/1000 ft outer diameter = 0.2 in. (contains 6 usable fiber strands). Minimum bend radius = 1 in.	JT 1412J (Times) and RG-11/U, 96 lb/1000 ft; RG-59/U, 32 lb/1000 ft. Twin Coax (CX-11230), 90 lb/1000 ft outside diameter; 0.48 in. (JT 1412J), 0.4 in. (RG-11/U), 0.24 in.; RG-59/U minimum bend radius = 4.8 in. (JT 1412J)	26 pair cable (CX-566), 293 lb/1000 ft
Crosstalk Isolation	80 to 95 dB/unit length (multi-fiber cable)	Typically 50 to 60 dB/unit length (bundled cables, individually shielded)	50 to 65 dB/unit length (MIL-STD-188C Requirements)
	Cost from \$0.90 per meter for uncabled waveguide. \$2.16 per meter for cabled fiber	\$0.30/m Times) \$0.91/m (CX-11230, Twin coax) \$0.21/m (RG-59/U) \$0.48/m (RG-11/U)	\$4/m (26 cable, CX-566)

### SECTION 3

#### THE ADVANTAGES AND LIMITATIONS OF AN OPTICAL WAVEGUIDE DATA BUS

Fiber-optics technology has matured rapidly in the past few years. Part of this growth has been spurred by the implementation of glass waveguide for long-haul telecommunication networks. Telecommunication networks were finally made possible by the tremendous improvement in the attenuation of glass waveguides (shown in Figure 2) and the accompanying improvement in fiber dispersion (shown in Figure 3).

Despite the advantages of fiber optics and although the basic technology is available, there are presently few operational fiber-optic data buses in existence. Several developmental fiber-optic data bus systems have been built as demonstration units. These couple four through eight users (terminals) at up to a 10-Mb/sec data rate.

The concepts of the design of a fiber-optic bus system are well known. The design is similar to the design of a point-to-point link in that a link optical power budget and a link rise time budget are initially required. These budgets determine the appropriate sources, fiber, and detector types required to meet the system performance goals. The power budget consists of calculations of worst-case optical power losses along the highest and lowest loss paths. The minimum received signal level (sensitivity) determines what combinations of bit rates and error rates are attainable with a particular bus design. Each optical receiver must be able to operate at all signal levels encountered from the highest to the lowest loss paths. The difference in loss between the highest and lowest loss paths (expressed in dB) is known as the optical signal range. The optical receiver sensitivity and the optical signal range required are important parameters associated with initial optical waveguide bus design.

Optical waveguide bus topologies are constructed from two basic designs: serial (shown in Figure 4) and parallel (Figure 5). Each has its particular advantages for the system designer.

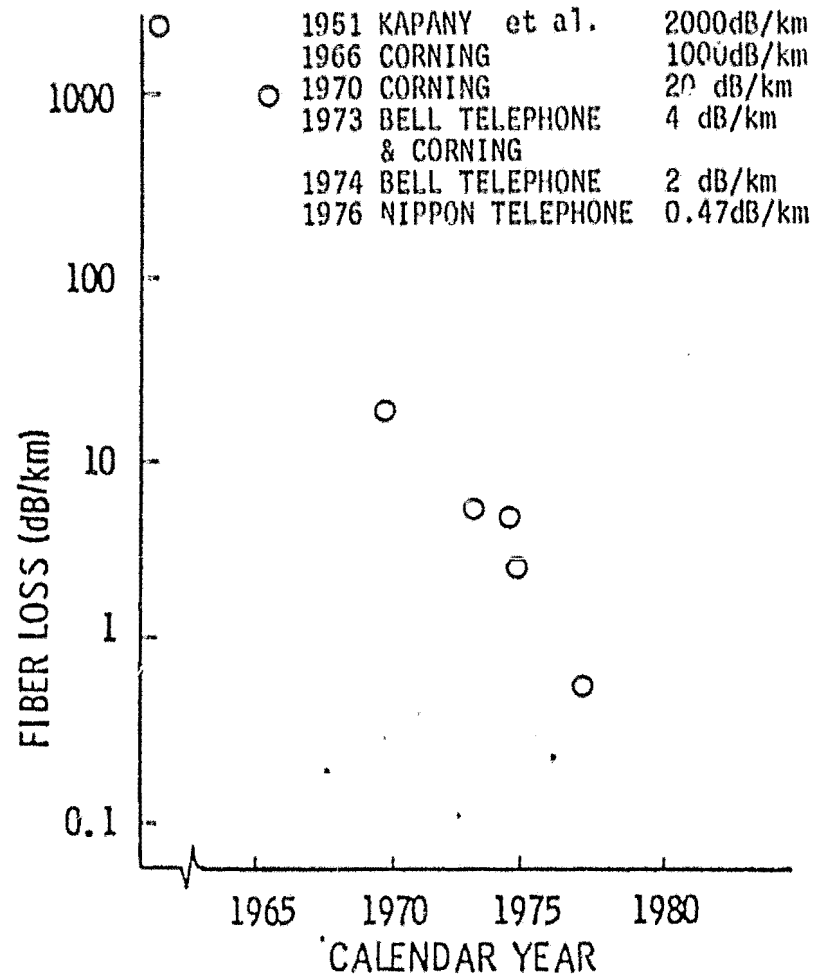


Figure 2. Optical waveguide attenuation has been dramatically reduced over the past twenty years.

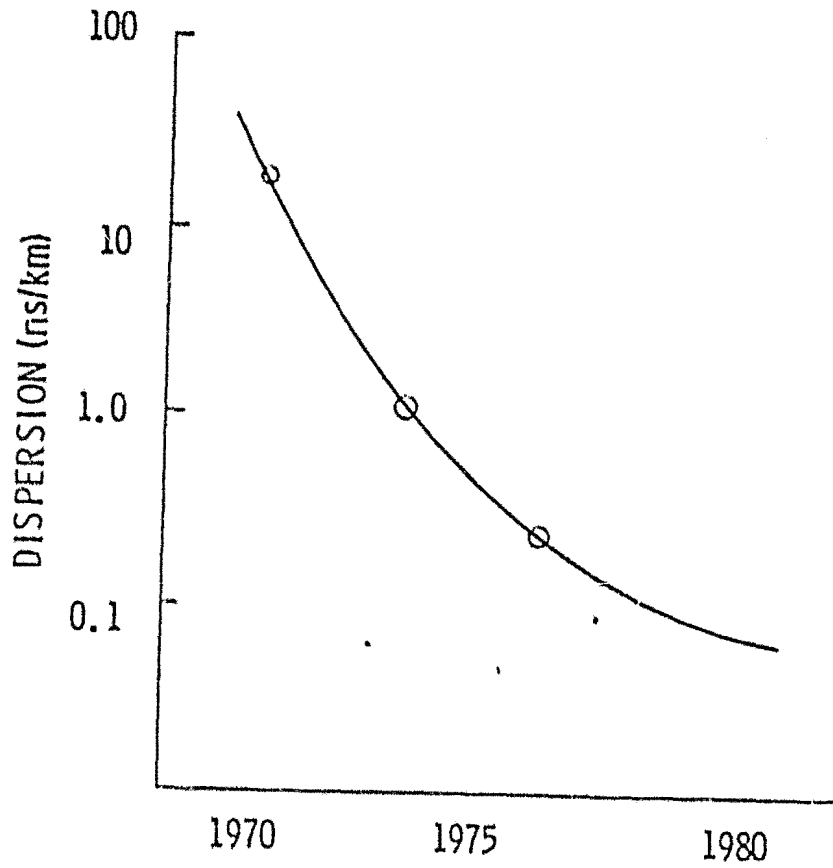


Figure 3. Dispersion in optical waveguide has been reduced by more than two orders of magnitude using graded-index multimode and single-mode fibers.

0113-11

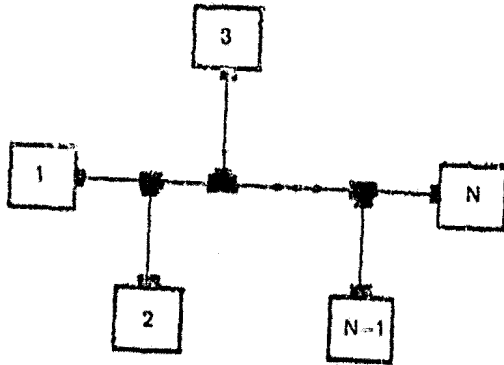
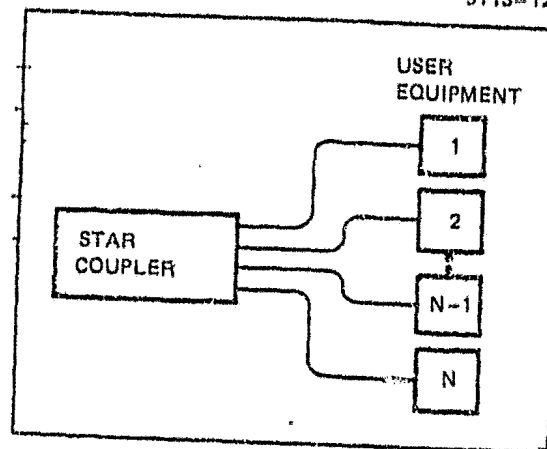


Figure 4. A serial data bus employing N access or Tee couplers.

0113-12

Figure 5. A parallel data bus employing a single N-port star coupler.



The serial bus has the advantage that additional terminals may be conveniently attached (assuming that adequate signal power is available). Also, for certain distributions of terminals, a significant reduction in the amount of required optical cable is possible. However, a single point failure could disable most of a multidrop bus.

An increase in the number of allowable terminals results from using a parallel bus. The graph of Figure 6 relates signal power available at each terminal to the number of terminals on the bus for both the serial and the parallel bus arrangements. Typical values of receiver sensitivity, coupler loss, and power input into the optical waveguide were used to generate the figure. A repeaterless bus requiring many terminals is clearly best implemented in parallel form.

Uniformity of signal distribution and the ability to handle many terminals makes the star topology attractive. By providing spare arms for the coupler, future growth can be accommodated. In addition, the parallel structure has the advantage of operating even if part of the bus is damaged. Unless the coupler itself is disabled, only the terminal on the inoperative leg will be functionally disconnected from the bus.

Terminals attached to a multidrop serial bus must be capable of handling a wide range of input signal levels. Signals arriving from distant couplers undergo repeated signal amplitude divisions and consequently are very weak. Signals arriving from nearby terminals are quite strong; hence, receivers must have a large dynamic range. Conversely, signal levels at each terminal of a parallel bus are nearly independent of the originating site. This reduces the dynamic range required in the receiver and simplifies the receiver's design.

To implement a particular optical waveguide data bus design, some type of multiple-access coupler is required. These couplers include Tee couplers, transmissive star couplers, reflective star couplers, and bifurcation devices. Active Tee and star couplers with built-in electrical repeaters add to the variety of couplers available. In most cases, these couplers are developmental. Few off-the-shelf units are available. Nonetheless, progress in the optical coupler area is so marked that off-the-shelf N-port transmissive star couplers are not far off in the

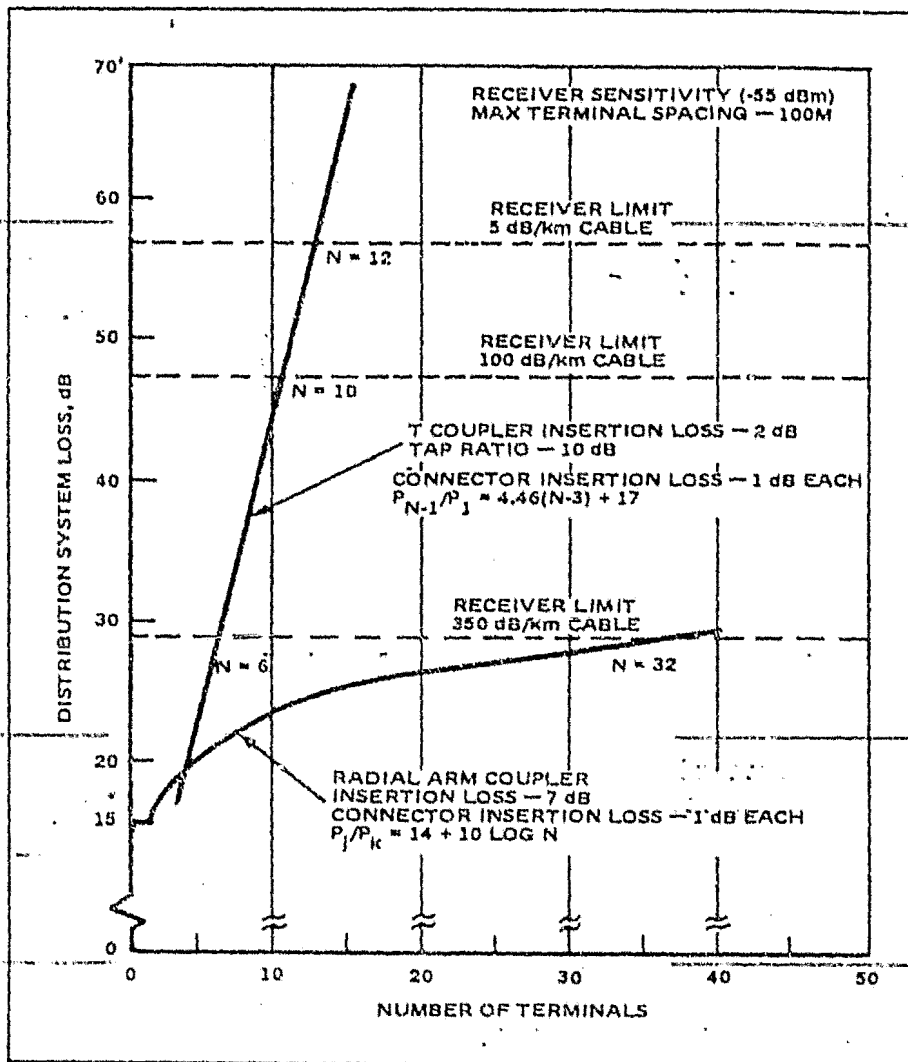


Figure 6. Typical distribution system loss plotted as a function of the number of terminals.

future and cannot legitimately be considered the limiting quantity in the 1980 plus timeframe.

On the other hand, limitations do exist in the amount of optical source power available from present LEDs and semiconductor laser sources. Source power is typically in the range of 300  $\mu$ W to several milliwatts. This power output is unlikely to increase substantially in the near future, especially for off-the-shelf components.

Since the trend in coaxial bus designs is towards higher data rates, it seems reasonable to expect that the demand for higher data rates, over longer buses and with more terminals, will continue. To optimize the bus data quality and traffic control, novel approaches to bus control will need to be investigated. Presently, Hughes is investigating the use of a decentralized bus control, in which control of an optical bus is passed on a serial time-shared basis and the protocol is designed to deal with terminal failures, removal or addition of a terminal (device) without interrupting bus performance, and other automatic bus recovery schemes.

The next-generation optical-waveguide bus design will require more attention to the communication aspects of bus designs, such as bus protocol, modulation, and error recovery, rather than to any specific optical component. This is not to say that component improvement is unimportant, only that it is not the pacing item for future optical-waveguide bus performance. Performance improvements will depend more on the development of bus interface standards and modules compatible with standard commercial and military type interfaces.

## SECTION 4

### TEE AND STAR COUPLERS

This section discusses the two most widely used passive couplers, the Tee (or access) coupler and the star coupler. Other potential geometries are mentioned briefly.

#### A. STAR COUPLERS

##### 1. Fused Fiber Star Coupler

The basic concept of this coupler is illustrated in Figure 7. From a black-box standpoint, there are  $N$  input ports, each designated by a unique unprimed number, and  $N$  output ports, each designated by a unique primed number. Power  $I_i$  is launched onto port  $i$ , and the power that exits from any of the  $2N$  ports is designated by  $O_j$  or  $O_j'$ . The taps are considered to be the  $N-1$  output ports exclusive of the bus (or launch) output port.

Below the stylized black box in Figure 7 is a list of the terms and the mathematical definitions that are used to characterize these devices. These definitions apply only when power is launched into only one of the  $N$  input ports; consequently, each of these terms must be computed for each of the  $N$  input ports. Furthermore, these devices must exhibit symmetry in their operation. So to completely characterize them, they must be considered with power launched into the primed ports. To this end, the last term, called coupler symmetry, is unique in that it singularly considers the effect of power launched in both directions. Note that each definition is preceded by a minus sign so that each will ultimately be positive. When a single number is given as the value of a particular term in Figure 7, the number will represent the average of the values received for power launched into all ports.

The basic design of the fused fiber coupler is illustrated in Figure 8. Two fibers are heated beyond the softening point of their cladding material and then stretched. This produces a biconically tapered region consisting of two longitudinal tapers separated by a



$I_i$  or  $I_i'$  is the power launched into port  $i$  or  $i'$  (bus or launch port)

$O_j$  or  $O_j'$  is the power which exits from port  $j$  or  $j'$

$A_{ij}$  is the fractional power at port  $j$  due to power launched into port  $i$ , i.e.  $A_{ij} = \frac{O_j}{I_i}$  ( $j$  or  $i$  may be primed)

$i, j, k = 1, 2, \dots, N$

$$\text{BUS RETURN LOSS (db)} = -10 \log_{10} [A_{ii}]$$

$$\text{TAP RETURN LOSS (db)} = -10 \log_{10} [A_{ij}] ; j \neq i$$

$$\text{BUS INSERTION LOSS (db)} = -10 \log_{10} [A_{ii}']$$

$$\text{TAP INSERTION LOSS (db)} = -10 \log_{10} [A_{ij}'] ; j \neq i$$

$$\text{TAP RATIO (db)} = -10 \log_{10} \left[ \frac{A_{ij}'}{A_{ii}'} \right] ; j \neq i$$

$$\text{COUPLING RATIO (db)} = -10 \log_{10} \left[ \frac{A_{ij}'}{\sum_k A_{ik}'} \right] ; j \neq i$$

$$\text{EXCESS LOSS (db)} = -10 \log_{10} \left[ \sum_k A_{ik}' \right]$$

$$\text{TAP UNIFORMITY (db)} = -10 \log_{10} \left[ \frac{A_{ij}'_{\min}}{A_{ij}'_{\max}} \right] ; j \neq i$$

$$\text{COUPLER SYMMETRY (db)} = -10 \log_{10} \left[ \frac{A_{ij}'}{A_{ji}'} \right]$$

Figure 7. A schematic of a fused fiber star coupler including the definitions of various coupler terms.

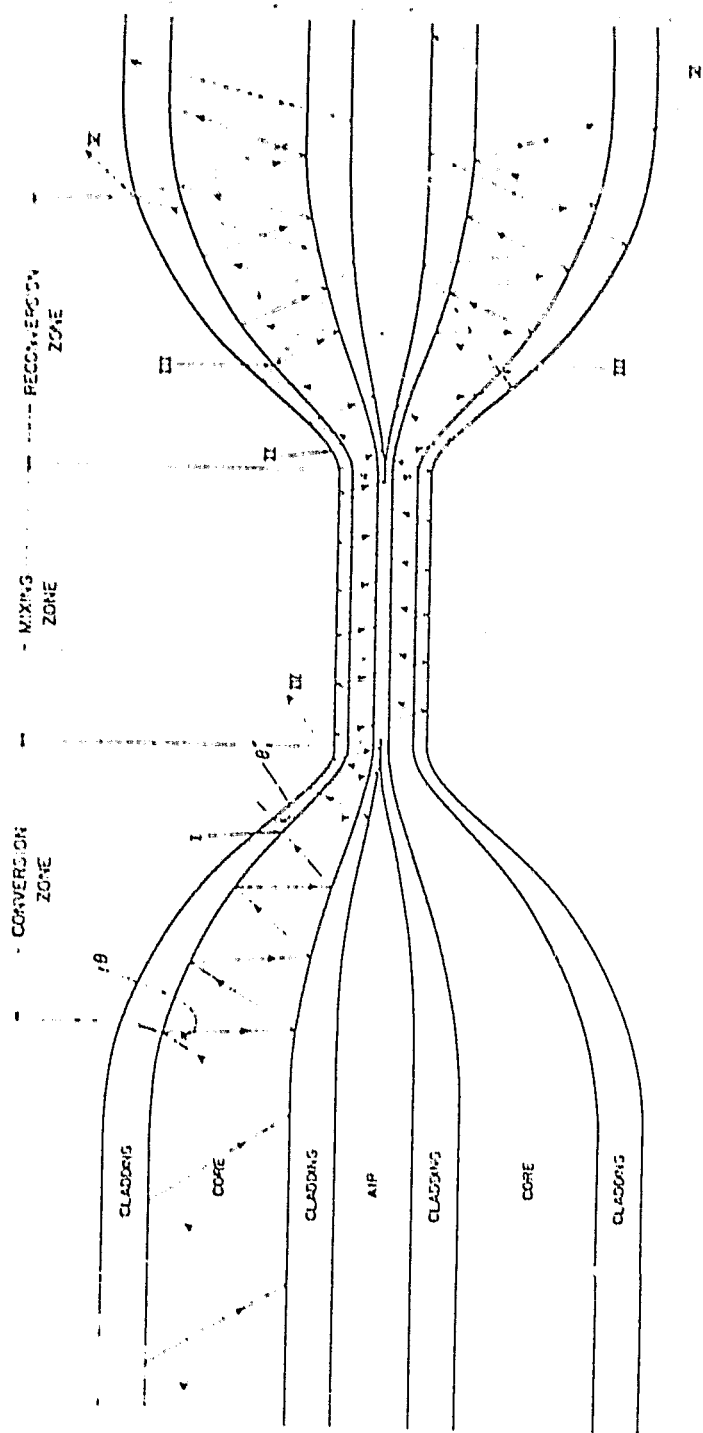


Figure 8. Configuration of the fused fiber coupler.

mixing zone. If the fibers are held in contact during heating and stretching, fusion of the cladding materials in and around the mixing zone will occur.

Since the dimensions of the optical structure in Figure 8 are much greater than one wavelength, a ray-optic (multimode) analysis is sufficient to describe the optical characteristics of these couplers. For simplicity, a step-index distribution is assumed in the optical fiber, but note that the results are directly applicable to graded core fibers.

Light enters the biconically tapered region from the left and is trapped in the core of one of the optical fibers. Ray-optic theory predicts a zig-zag path, which is denoted by the solid lines in Figure 8. The effect of the first of the tapered zones is to cause a steadily decreasing angle  $\theta$ , where  $\theta$  is defined as the angle between the ray and the normal to the core-cladding interface. At some point (denoted by I in Figure 8),  $\theta$  is sufficiently reduced to be below the critical angle for total internal reflection at the core-cladding interface. The light is no longer trapped within the core and is converted to a cladding mode, trapped within the cladding of the fiber by the cladding-air interface. This cladding mode propagates to the mixing zone, where coupling to the other fiber(s) occurs.

In the mixing zone, the light mixes nearly equally throughout the joint cladding and is approximately evenly divided among the individual claddings when the fibers separate at the end of the mixing zone (Point II in Figure 8). At this point, the light enters the second tapered zone of the biconically tapered region. From symmetry, the process of core-to-cladding power conversion, which occurred in the first tapered zone, is reversed in the second. At Point III, power is reconverted to the core, where it remains as it exits from the conically tapered region. Since the available power was split among all of the output fibers at the end of the mixing zone, cladding-to-core reconversion occurs in all fibers, and the goal of a fiber-optic coupler has been achieved.

The above description is greatly simplified. In actual practice, the two tapered zones and the fused mixing zone overlap. Consequently, core-to-cladding and cladding-to-core conversions are spatially interspersed

with mixing in the joint cladding. The degree to which this occurs and its effects on the optical characteristics of fused fiber couplers are presently under investigation and have yet to be completely determined.

There are two basic mechanisms that contribute to losses in the fused fiber coupler: (1) overconversion in the tapered conversion zone, and (2) insufficient reconversion in the tapered reconversion zone. Scattering losses are also present but are negligible when compared to those listed above.

Overconversion is caused by the same mechanism that causes light to be converted from core to cladding modes. Following Point I (in Figure 8), power is trapped in the cladding by total internal reflection at the cladding-air interface. However, since the taper continues after Point I, conversion continues to occur, causing a decrease in the angle  $\theta'$ . If the taper continues too far and  $\theta'$  is reduced below the critical angle for the cladding-air interface, then light will couple out of the cladding into the surrounding medium, where it is lost.

The same effect can occur when these devices are encapsulated. Since any practical encapsulant will have an index of refraction greater than that of air ( $N_{\text{air}} = 1.0$ ), encapsulating the device will reduce the critical angle at the outer cladding boundary. Therefore, rather than reducing  $\theta'$  below the critical angle, encapsulation can have the effect of raising the critical angle to the point where it is above  $\theta'$ . In either case, the result is overconversion at Point IV and losses due to coupling into the surrounding medium.

The second major loss mechanism is insufficient reconversion in the tapered reconversion zone. Experimental evidence indicates that, under certain conditions, the tapered conversion and reconversion zones are not symmetric. In other words, while their beginning and ending diameters are the same, the two tapers occur over different longitudinal distances, producing different taper angles. This asymmetry may be the cause of insufficient or improper reconversion in the tapered reconversion zone. The result would be power that remains in the cladding after passing through the tapered reconversion zone. These cladding modes are illustrated by the arrows in the cladding following Point III in Figure 8.

## 2. Bulk Optical Reflection Star Couplers

The bulk optical star, or radial, coupler concept is shown in Figure 9. Several fibers are attached to one face of a mixing rod. Light enters the mixing rod, which is long enough to allow the light to become approximately uniformly distributed after being reflected and returned to the fiber end faces. Since each fiber is uniformly illuminated, each receives  $1/n$  of the power, where  $n$  is the number of fibers.

In addition to the splitting loss, this coupler exhibits packing fraction loss. The packing fraction is a geometric loss factor that is due to the difference between the cross-sectional area of the core and that of the mixing rod. For example, Figure 10 shows two packing arrangements, hexagonal close-pack and linear close-pack. The packing fraction for the hexagonal close-pack is given by:

$$F_{\text{hex}} = \frac{N_d^2 D_{\text{core}}^2}{N D_{\text{clad}}^2} \quad (2)$$

where

$N$  = the total number of fibers (3, 7, 19, 37, 61, etc.)

$N_d$  = number of fibers along the smallest diameter circle containing all fibers

$D_{\text{core}}$  = diameter of the core

$D_{\text{clad}}$  = diameter of the cladding.

The packing fraction for the linear close-pack is

$$F_{\text{lin}} = \frac{4}{\pi} \frac{D_{\text{clad}}^2}{D_{\text{core}}^2} \quad (3)$$

Clearly, large core to clad ratios and/or removal of the cladding minimizes the packing fraction loss. In the case where  $D_{\text{clad}}/D_{\text{core}}$  is

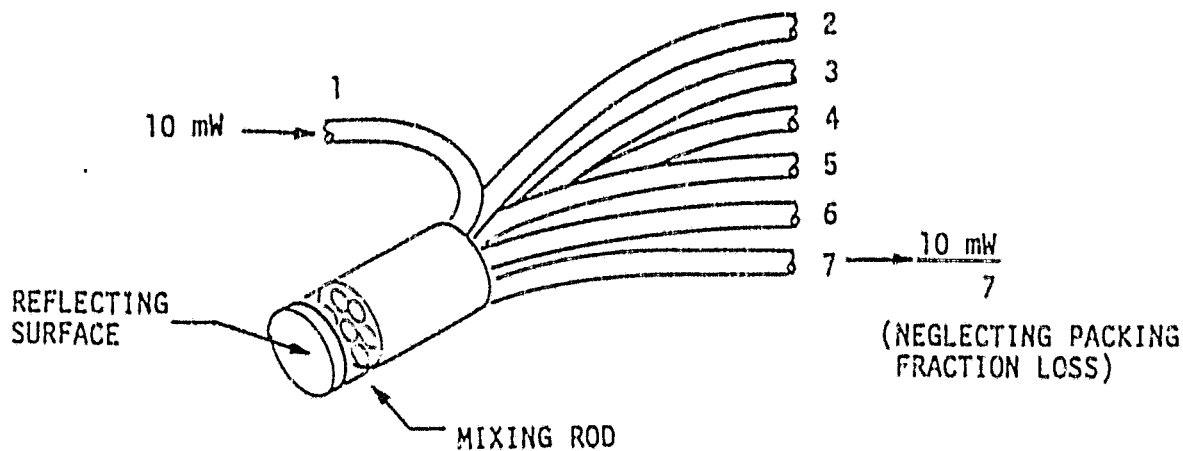


Figure 9. A reflective star may be constructed by attaching fibers to one end of a mixing rod with a reflective surface on the other end.



Figure 10. Packing fraction loss is due to the area mismatch between the fiber cores and the area of the mixing rod.

approximately one, the hexagonal close-pack yields losses of 1.09, 1.19, 1.22, and 1.23 dB, respectively, for the 7, 19, 37, and 61 fiber configurations, while the linear close pack is a constant 1.05 dB. In addition to the packing fraction loss, there is usually an excess loss that relates to fiber attachment, mixing rod imperfections, and general construction technique.

The transfer matrix for the reflective star may be approximated by

$$a_{ij} \approx (F_{\text{losses}})^{\frac{1}{N}} \quad i, j = 1, N, \quad (4)$$

where

$F_{\text{losses}}$  = the fraction transmission due to packing fraction and excess loss

$N$  = number of radial arms.

This transfer matrix is slightly over-simplified. In reality, there are variations from element to element caused by nonuniform light distribution and by variations in fiber attachment. In determining receiver dynamic range, these variations are important and must be included.

### 3. Bulk Optical Transmission Star Coupler

Another star configuration is the transmission star shown in Figure 11. Here one side serves as input ports to the mixing rod and the other serves as output ports. The rod must be long enough (several centimeters) so mixing is complete at the output side of the rod. The transfer matrix for the transmissive star is approximately

$$a_{ij} \approx (F_{\text{losses}}) \frac{1}{N} \quad i, j = 1, N \quad . \quad (5)$$

9113-18

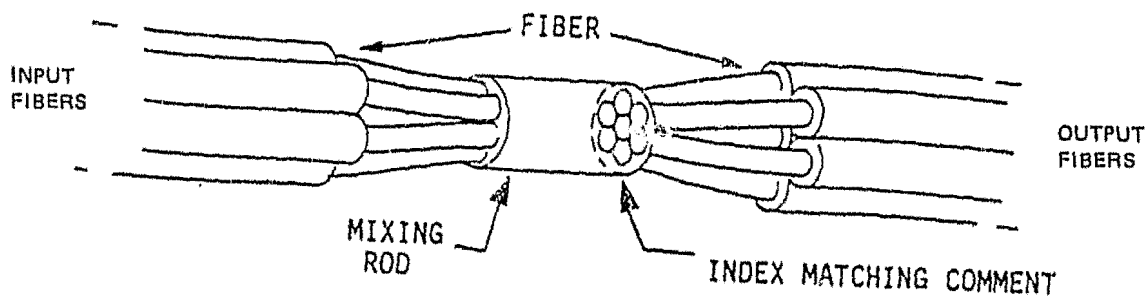


Figure 11. The transmission star has fibers attached at each end of the mixing rod. One end serves for optical inputs, the other for optical outputs.

#### 4. Planar Star Coupler

An alternative to bulk star coupler design uses planar geometry. Planar geometry is well suited to applications where a limited number of fibers are to be coupled. By using a planar structure design, the many advantages of photolithographic processing technology apply. A schematic of a reflective planar star coupler design is shown in Figure 12. Multi-mode fibers are held in alignment grooves formed by selective etching or embossing techniques. Because of the high precision and reproducibility with which photolithographic and embossing techniques can be performed, these alignment grooves produce an alignment accuracy which is extremely difficult to attain with a conventional approach. In addition, each fiber may be readily examined and adjusted individually without disturbing the other fibers. The fibers are butt coupled to channel waveguides. The channel waveguides serve as interconnecting links with the mixing region. Each channel guide is expanded into a mixing region. The mixing region allows the fields to expand so that the radiation reflected from the mirrored end surface approximately uniformly illuminates the collection horns. A transmissive star may be produced by replacing the end reflector at the right of Figure 12 with a mirror image of the pattern. The transfer matrices for the planar star configurations are identical in form to those of conventional star couplers (Eq. 5).

#### B. TEE COUPLERS

##### 1. Fused Fiber Tee Coupler

The optical Tee, or access, coupler allows a tap, or "drop," to be made from the main optical bus. A common method for producing these couplers is to stretch two single fibers as they are heated and the claddings fuse together. This procedure forms a biconical taper. As light enters the decreasing taper, guided modes are converted to cladding modes. During transmission through the fused region, a portion of the optical power in the cladding modes is exchanged between the fibers. The cladding modes are then converted back to core-guided modes as the

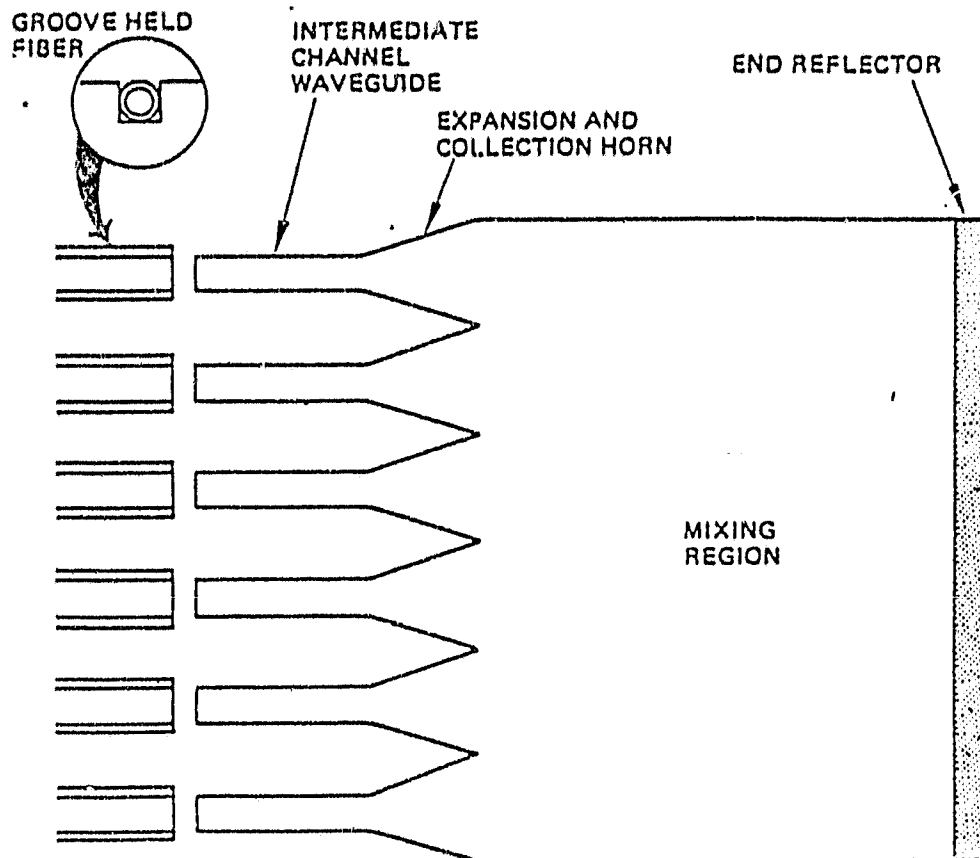


Figure 12. A planar star coupler.

taper increases at the output of the junction. During coupler construction, various parameters are controlled to alter the fraction of the power that is removed from the bus.

Figure 13 shows the coupler as a four-port device and defines variables. Ports 1 and 3 are on one fiber, and ports 2 and 4 on the other. The fraction of the input power  $P_{in}$  that exits at port  $j$  and that was launched into port  $i$  is denoted by  $a_{ij}$ . In the ideal case, shown in Figure 13,  $a_{11}$ ,  $a_{21}$ , and  $e_1$  would all be zero and the sum of  $a_{31}$  and  $a_{41}$  would be one. In any real case, there is excess loss  $e_1$  when power is launched into port  $i$ . By conservation of energy, we have:

$$\sum_{j=1}^4 a_{ij} + e_j = 1 \quad \text{for } i = 1, 2, 3, 4 \quad (6)$$

The parameters  $a_{ij}$ , where  $i$  is not equal to  $j$ , are easily measured. The power measurements are made external to a cleaved fiber end. Since the normalizing (launch) power is finally measured by cleaving the fiber at the input port, the coefficients are determined directly. Mode strippers are used during the measurement process. For example, if power is

9113-20

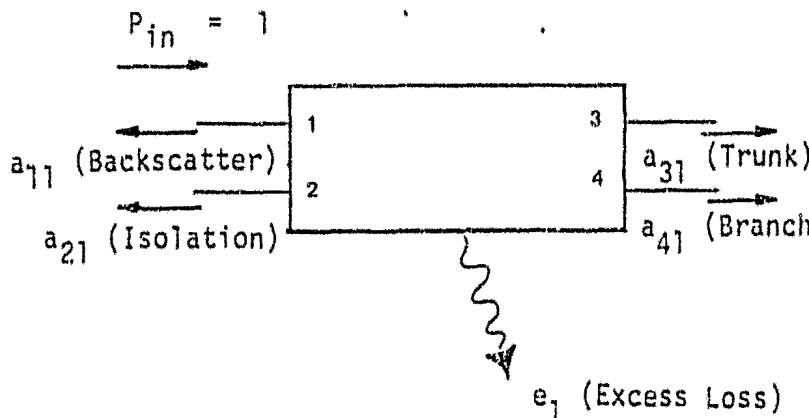


Figure 13. The generalized four-port optical Tee coupler.

launched into port 1,  $a_{21}$  is measured with ports 3 and 4 terminated with an index-matching fluid to prevent reflections. This coefficient, called coupler isolation, is at least -35 dB down from the input port power. The output coefficients  $a_{31}$  and  $a_{41}$  are measured similarly. The coupler is characterized by repeating the measurements using each port as an input.

The isolation coefficients are non-zero due to bulk fiber backscatter and fused junction imperfection. The same basic mechanisms are at play to produce a non-zero  $a_{ii}$ . Since these diagonal elements are difficult to measure, they are assumed to be approximately equal to the isolation coefficients.

The isolation coefficient is a function of the tap ratio and also of coupler fabrication. The value of -35 dB is a worst case and is noted only for equal power division. This coefficient decreases as the tap ratio increases and reaches a value of less than -50 dB for 15-dB couplers.

All the measurements performed on the coupler can be combined into a transfer matrix which completely describes the couplers. The transfer matrix is:

$$a_{ij} = \begin{bmatrix} \delta & \delta & \alpha & \beta \\ \delta & \delta & b & a \\ \alpha & b & \delta & \delta \\ \beta & a & \delta & \delta \end{bmatrix}, \quad (7)$$

where  $\alpha(a)$  is the insertion loss of the trunk,  $\beta(b)$  is the insertion loss of the tap, and  $\delta$  is the backscatter coefficient (or the isolation).

Experimentally,  $a_{ij}$  is found to be approximately equal to  $a_{ji}$ , as required by reciprocity. The equality of the small elements represented by  $\delta$  is an approximation for the backscatter and isolation parameters.

Furthermore, a good coupler exhibits  $a \approx \alpha$  and  $b \approx \beta$  due to symmetry and homogeneity of excess loss mechanisms. We use

$$a_{ij} = \begin{bmatrix} \delta & \delta & \alpha & \beta \\ \delta & \delta & \beta & \alpha \\ \alpha & \beta & \delta & \delta \\ \beta & \alpha & \delta & \delta \end{bmatrix} \quad (8)$$

as a first-order approximation supported by experimental measurements. Typical parameters for an equal power division coupler are  $\alpha = 0.38$ ,  $\beta = 0.42$ , and  $\delta = 3 \times 10^{-4}$ . The measured tap ratio and excess loss for a set of 36 fused-Tee couplers are shown in Figure 14.

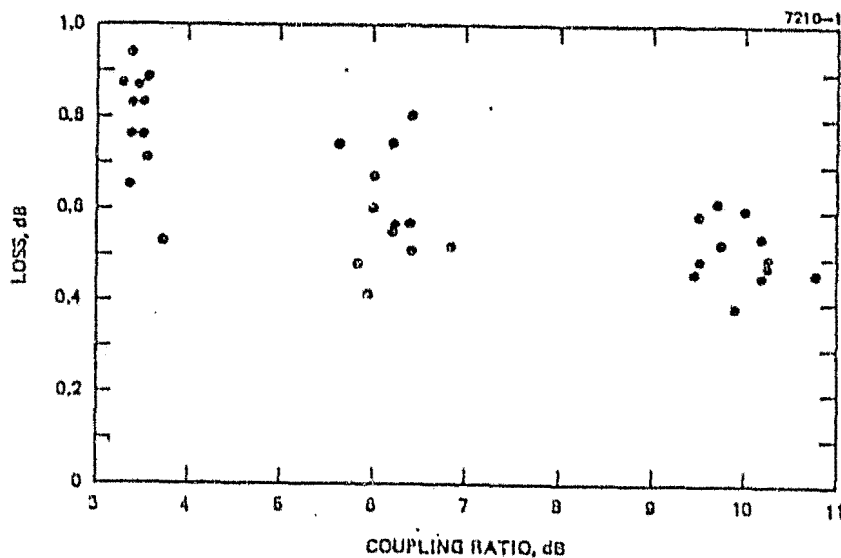


Figure 14. Excess loss plotted as a function of tap ratio for 36 fused-Tee couplers.

## 2. Planar Y Coupler

Planar optical access couplers are based on a proprietary masking and diffusion process. The concept is illustrated in Figure 15. The process holds great promise for low-cost, well-controlled, mass-producible, multi-mode optical components. These devices have been demonstrated in the laboratory.

Since the channel is determined by a masking operation, a wide variety of geometries may be fabricated. The tap ratio of a planar Y with equal area ports is established by the angle between the two arms. If the excess loss and backscatter are neglected, the transfer matrix for the device is:

$$A_3 \cong \begin{bmatrix} 0 & 1-\alpha & \alpha \\ 1-\alpha & 0 & 0 \\ \alpha & 0 & 0 \end{bmatrix}, \quad (9)$$

where  $\alpha$  is the fraction of the power that is tapped from the bus.

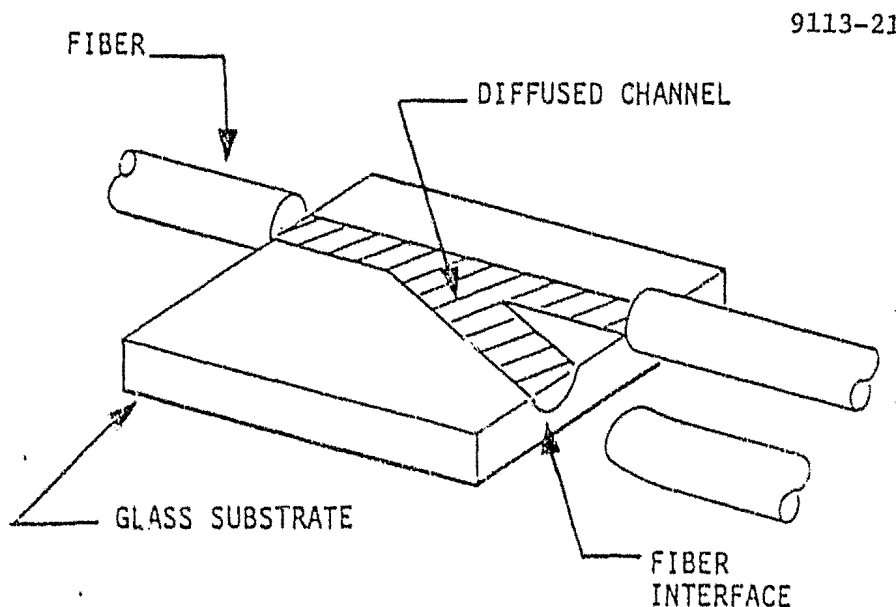


Figure 15. A concept for production of planar optical Tee couplers.

### 3. Planar Tee Coupler

Three planar Y couplers may be combined on a single substrate to form a planar Tee, as indicated in Figure 16. The transfer matrix for this configuration is

$$A_4 \approx \begin{bmatrix} 0 & (1-\beta)(1-\alpha) & \gamma\alpha \\ (1-\alpha)(1-\beta) & 0 & (1-\gamma)\beta \\ \alpha\gamma & \beta(1-\gamma) & 0 \end{bmatrix}, \quad (10)$$

where the fraction of the power tapped at each Y is given by  $\alpha$ ,  $\beta$ , and  $\gamma$  as indicated.

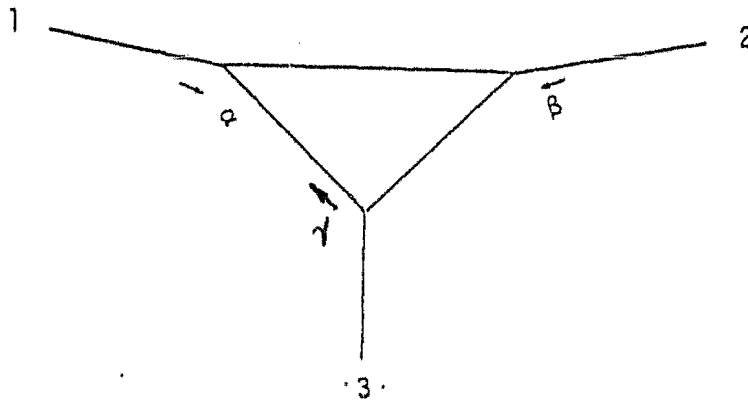


Figure 16. Three planar Y couplers are combined to form a planar Tee coupler.

## SECTION 5

### A 32-PORT TRANSMISSIVE STAR COUPLER SYSTEM FOR SPACECRAFT APPLICATION

This section analyzes a simple 32-port star system. The results show that a LED source and PIN diode detector combination can provide a sufficient margin to successfully operate a 10 Mb/sec NRZ-coded data bus at a  $10^{-11}$  bit-error-rate (BER). Such a system is expected to consume less than 380 mW of electrical power, making it a prime candidate for spacecraft applications.

The system analyzed is the simple one shown in Figure 17. It consists of:

- A 32-port transmissive star coupler
- 32 sources and associated driver electronics
- 32 detectors and associated receivers
- 128 connectors (one connector at each port of the star coupler, one connector near each source, and one connector near each receiver).

Both the optical and the electrical power budgets are determined.

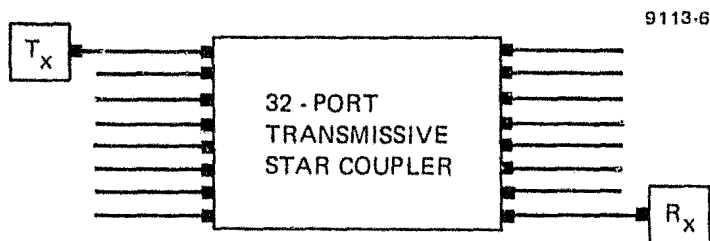


Figure 17. A basic 32-port star data bus. Each ■ indicates a single fiber connector.

Before analyzing the actual system, the theoretical value of detected power required to achieve a given BER is determined. The theoretical analysis begins with the equivalent circuit of a photodetector and its associated load resistor, as shown in Figure 18. In this model,  $I_{sig}$  is the primary (signal) photocurrent, which is related to the optical signal power  $P_{sig}$  by the detector responsivity  $r$  according to

$$\begin{aligned}
 I_{sig} &= r P_{sig} \\
 &= \frac{\eta e}{h\nu} P_{sig} \quad , \quad (11)
 \end{aligned}$$

where

$\eta$  = quantum efficiency

$e$  = electronic charge

$h$  = Planck's constant

$\nu$  = photon frequency.

All noise sources are assumed to be double-sided white noise sources. The current  $i_s^2$  is the mean-square shot-noise current, which is related

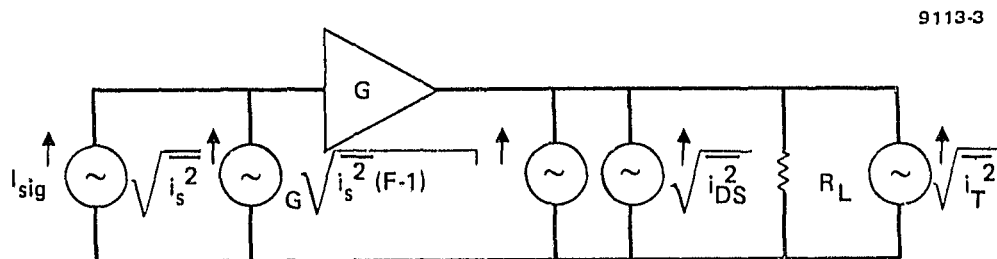


Figure 18. An equivalent circuit of a general photodetector and its load resistor  $R_L$ .

to the total current  $I_T$  flowing in the detector and to the detector bandwidth  $B$  through

$$\overline{i_s}^2 = eI_T B \quad . \quad (12)$$

The total detector current consists of three parts:

- Signal photocurrent  $I_{sig}$
- Photocurrent generated by any optical background,  $I_B$
- Bulk dark current  $I_{DB}$ .

In any well-designed fiber-optic system, the optical background current  $I_B$  is negligible; hence, it is neglected in the following analysis. The mean-square shot-noise current can be written as

$$\overline{i_s}^2 = e (I_{DB} + r P_{sig}) B \quad . \quad (13)$$

The equivalent circuit of Figure 18 allows for intrinsic gain  $G$  in the detector. If there is intrinsic gain, as in an avalanche photodiode, there is an excess noise factor  $F$ . The excess noise factor is empirically determined to be dependent on the intrinsic gain according to a power law

$$F = G^x \quad , \quad (14)$$

where  $x$  is an empirically determined constant.

The two remaining noise sources are surface dark current  $I_{DS}$  and Johnson (thermal) noise. Noise due to surface dark current is calculated using the formula

$$\overline{i_{DS}}^2 = eI_{DS} B \quad . \quad (15)$$

Thermal noise is found from

$$\overline{i_t}^2 = kTB/R_L \quad , \quad (16)$$

where  $k$  is Boltzman's constant,  $T$  is the absolute temperature, and  $R_L$  is the load resistance.

Summing all these noise currents, we find the total mean-square noise current to be:

$$\bar{i}_n^2 = \left[ e (I_{DB} + rP_{sig}) G^2 F + eI_{DS} + \frac{2kT}{R_L} \right] B \quad (17)$$

The signal current is

$$I_S = GrP_{sig} \quad (18)$$

The probability of an error occurring can be calculated. The probability of an error occurring while detecting a zero is

$$\begin{aligned} P_e(0) &= \left( 2\sigma_o^2 \right)^{-1/2} \int_{I_T}^{\infty} \exp\left( \frac{-i^2}{2\sigma_o^2} \right) di \\ &= \frac{1}{2} \operatorname{erfc} \left( \frac{I_T}{\sqrt{2}\sigma_o} \right) \quad , \end{aligned} \quad (19)$$

where

$$\sigma_o^2 = \left( eI_{DB} G^2 F + eI_{DS} + \frac{2kT}{R_L} \right) B \quad , \quad (20)$$

and  $\operatorname{erfc}(x)$  is the complementary error function of argument  $x$ . The probability of an error occurring while detecting a one is

$$\begin{aligned}
P_e(1) &= \left(2\pi\sigma_1^2\right)^{-1/2} \int_{-\infty}^{I_T} \exp\left\{-\frac{(i - I_s)^2}{2\sigma_1^2}\right\} di \\
&= \frac{1}{2} \operatorname{erfc}\left(\frac{I_s - I_T}{\sqrt{2}\sigma_1}\right) , \tag{21}
\end{aligned}$$

where

$$\sigma_1^2 = \sigma_o^2 + rP_{\text{sig}} eG^2 \text{FB} . \tag{22}$$

The simplest type of detection scheme is to sample the received signal and compare it to a threshold level. The threshold level is calculated by requiring an equal number of errors when detecting ones as when detecting zeros. This occurs when

$$\frac{I_T}{\sigma_o} = \frac{I_s}{\sigma_1 + \sigma_o} \equiv Q . \tag{23}$$

Substituting Eq. 23 into Eq. 19 yields the probability of error as a function of the Q parameter:

$$P_e(0) = \frac{1}{2} \operatorname{erfc}\left(\frac{Q}{\sqrt{2}}\right) . \tag{24}$$

This functional dependence is plotted in Figure 19. Substituting Eq. 18 into Eq. 23 and assuming a 50% duty factor we find the average signal power required to maintain a given probability of error to be

$$\bar{P} = \left(\frac{Q}{2r}\right) \left(eQ\text{FB} + \frac{2}{G} \sigma_o\right) . \tag{25}$$

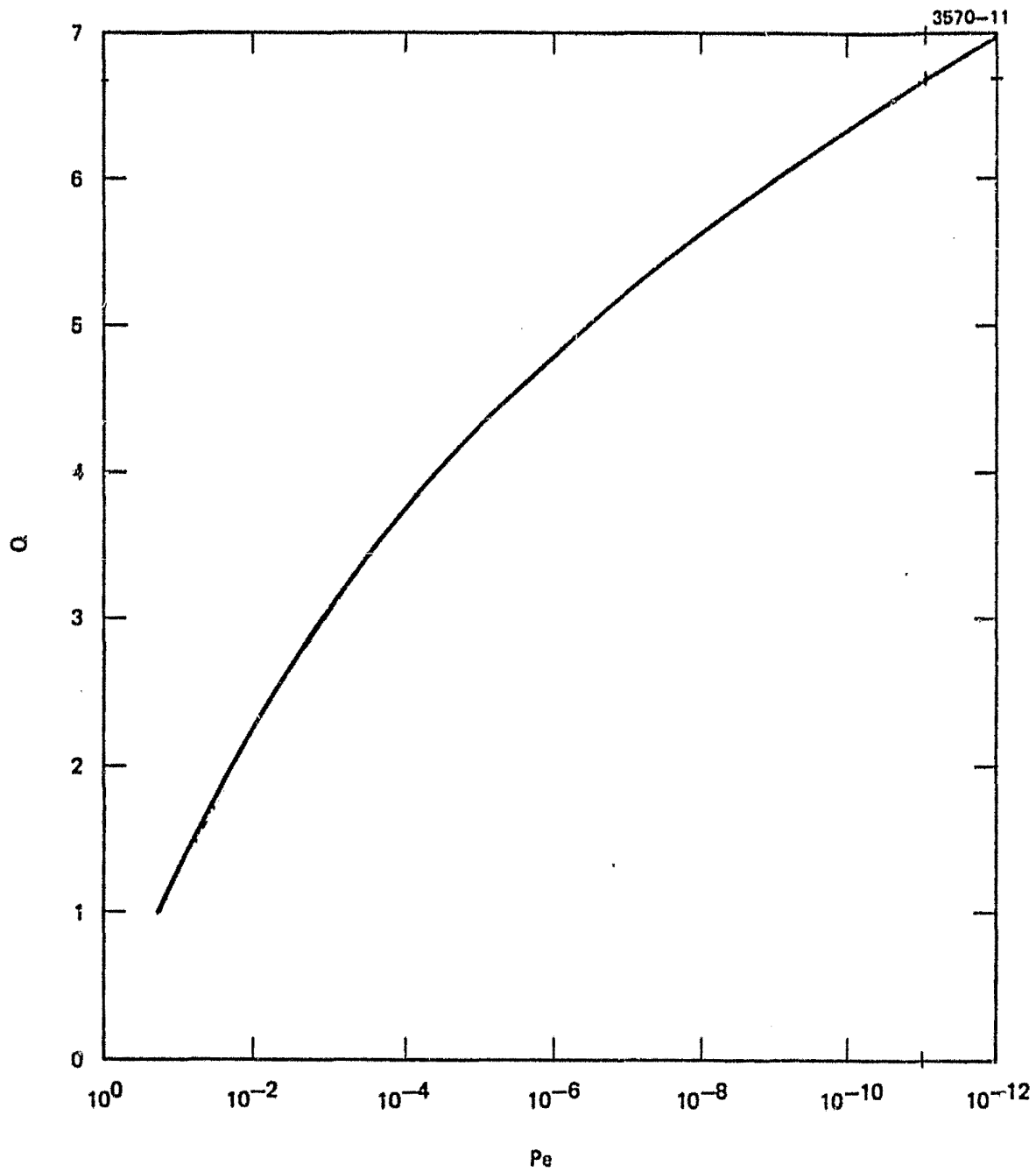


Figure 19. Probability of error from Eq. 25.

This result, the main one from this analysis, can be used to estimate the performance of a receiver. A typical commercially available PIN diode detector is the HP-5082-4205. This detector is characterized by:

- Responsivity 0.9 A/W
- Risetime  $< 1$  nsec
- NEP  $1.4 \times 10^{-14}$  W/ $\sqrt{\text{Hz}}$
- Dark current 0.15 nA at -10 V bias
- Effective area  $3 \times 10^{-3}$  cm<sup>2</sup> .

Since this is a PIN diode, there is no intrinsic gain; hence, both G and F are unity. Substituting into Eq. 20 and assuming a 10-MHz bandwidth yields an rms noise current  $\sigma_o$  of  $2 \times 10^{-9}$  A. Substituting this result into Eq. 25 gives the average signal power required to maintain a  $10^{-11}$  BER. That average signal power is  $2.8 \times 10^{-8}$  W, or -46 dBm.

#### A. OPTICAL POWER BUDGET

The first step in the design of a fiber system is to calculate the expected distribution system losses and compare those losses with the available power margin. Theoretically, we expect to be able to receive 10 Mbit/sec NRZ data at a  $10^{-11}$  BER if we have -46 dBm of optical power falling on an optimized PIN diode receiver. Practically speaking, Hughes has built receivers that provide  $10^{-11}$  BER performance if -42 dBm of signal power is available. A typical LED source (such as the Laser Diode Laboratories IRE-150) provides +2 dBm; consequently, the distribution system can consume not more than 44 dB.

The transmission star system shown in Figure 17 contains several attenuation sources, including:

- Input coupling loss I given by:

$$I = 10 \log \left( \frac{A_{\text{source}}}{A_{\text{core}}} \frac{2}{(n+1)(\text{NA})^2} \right), \quad A_{\text{source}} \leq A_{\text{core}}$$

$$= 10 \log \left( \frac{2}{(n+1)(\text{NA})^2} \right), \quad A_{\text{source}} > A_{\text{core}} \quad (26)$$

where  $A_{\text{source}}$  and  $A_{\text{core}}$  are the cross-sectional areas of the source and fiber cores, respectively;  $n$  is the refractive index; and  $NA$  is the numerical aperture.

- A connector insertion loss  $C$  occurs at four points in each signal path. For Deutsch single-fiber connectors, this loss is  $0.7 + 0.2$  dB assuming graded-index fiber is used.
- Fiber attenuation  $A$  given by:

$$A = \alpha L , \quad (27)$$

where  $\alpha$  is the fiber attenuation coefficient, and  $L$  is the length of the system.

- Star coupler insertion loss  $S$  given by:

$$S = 10 \log M , \quad (28)$$

where  $M$  is the number of ports in the star coupler.

- Star coupler excess loss  $E$  is difficult to calculate and consequently is usually determined empirically.
- There will be an additional  $N$  dB of loss margin to provide for the degradation of the source as it ages, port-to-port variation in coupled signal power, output coupling loss, etc.

The total distribution system loss  $T$  can be found by adding the six individual contributions,

$$T = I + N + C + A + S + E . \quad (29)$$

Notice that the greatest improvement in efficiency is possible in input coupling. Eq. 26 indicates that minimum input coupling loss occurs for a source with cross-sectional area matching that of the core of the fiber. It also shows that a high  $NA$  and/or high core index fiber reduces the input coupling loss.

For purposes of estimating system performance, three different source, detector, and fiber combinations are considered:

- (1) Laser Diode Laboratories IRE-150 LED source, HP-5082-4205 PIN diode detector, and QPC SI-300 plastic-clad silica fiber.
- (2) Bell-Northern 40-3-30-3 LED source with fiber pigtail, HP-5082-4205 PIN diode detector, and Corning 1025 fiber.
- (3) Hitachi HLP-2400 laser diode source, HP-5082-4205 PIN diode detector, and Corning 1025 fiber.

The relevant specifications of each of these components are listed below.

- Laser Diode Laboratories IRE-150 LED
  - Source wavelength 820 nm
  - Minimum output power 1 mW at 100 mA
  - Source area 230 by 230  $\mu\text{m}$
  - Risetime 7 nsec
- HP 5082-4205 PIN diode
  - Responsivity 0.5 A/W
  - Risetime < 1 nsec
  - NEP  $1.4 \times 10^{-14}$  W/ $\sqrt{\text{Hz}}$
  - Dark current 0.15 nA at -10 V bias
  - Effective area  $3 \times 10^{-3}$   $\text{cm}^2$
- QPC SI-300 plastic-clad silica fiber
  - Core diameter 300  $\mu\text{m}$
  - NA 0.35
  - Core index 1.46
  - Bandwidth 20 MHz-km
  - Attenuation < 3.5 dB/km at 0.85  $\mu\text{m}$

- Bell-Northern 40-3-30-3 LED source with integral fiber pigtail

Power output from pigtail 300  $\mu$ W at 150 mA

Risetime  $\leq$  12 nsec

Fiber core diameter 100  $\mu$ m

- Corning 1025 fiber

Core diameter 85  $\mu$ m

NA 0.18

Core index 1.48

Bandwidth 20 MHz-km

Attenuation  $\leq$  10 dB/km at 820  $\mu$ m

- Hitachi HLP-2400 laser diode

Source wavelength 820 nm

Minimum output power 1 mW

Source area 1 x 1  $\mu$ m

Risetime  $\leq$  500 psec .

In addition to sources, detectors, and fiber, this system will require single-fiber connectors and star couplers. The best single-fiber connectors commercially available today are Deutsch connectors. They are quoted at  $0.7 \pm 0.2$  dB insertion loss when typical graded-index fiber is used.<sup>1</sup>

Star couplers are currently under intense development and prototypes are coming onto the commercial marketplace. At least two types of coupler are being investigated: planar and fused.<sup>2,3</sup> The planar star coupler is manufactured on a glass slide using standard photolithographic techniques to delineate waveguides. Fused star couplers are made by melting several fibers together while simultaneously pulling on them to taper the fused region. Typical performance of planar and fused star couplers excited with a HeNe laser are presented in Tables 2 and 3, respectively.

Table 2. Typical Planar Star Coupler Performance

Input Port	Insertion Loss, dB								Excess Loss, dB	Mean Port-to-Port Insertion Loss, dB	Standard Deviation of Port-to-Port Insertion Loss, dB
	Output Port										
	1	2	3	4	5	6	7	8			
1	19.1	21.0	19.5	23.0	17.2	15.2	15.9	25.5	9.4	19.5	±3.5
2	17.8	17.9	19.1	15.7	21.0	16.9	18.7	21.4	9.2	18.6	±1.9
3	25.2	23.4	20.8	17.9	16.7	19.2	19.3	20.5	10.6	20.4	±2.8
4	27.0	26.4	25.4	23.1	18.7	16.4	17.9	17.6	10.9	21.6	±4.4
5	19.0	20.2	20.0	22.4	20.8	20.5	20.6	18.8	11.1	20.3	±1.1
6	20.7	19.9	20.0	22.5	20.6	20.8	19.1	18.6	11.1	20.3	±1.2
7	14.6	18.2	21.6	21.8	22.2	22.1	23.5	23.1	10.7	20.9	±3.0
8	24.6	14.6	18.2	21.9	22.4	23.3	23.2	21.7	10.9	21.2	±3.3
									10.5 (Average)	20.3 (Average)	±2.8 (Average)

47

Table 3. Typical Fused Star Coupler Performance

Input Port	Insertion Loss, dB								Excess Loss, dB	Mean Port-to-Port Insertion Loss, dB	Standard Deviation of Port-to-Port Insertion Loss, dB
	Output Port										
	1	2	3	4	5	6	7	8			
1	10.2	11.7	11.9	11.3	11.5	11.5	11.7	11.5	2.3	11.4	0.5
2	12.3	10.4	12.9	12.2	13.1	12.3	12.8	12.9	3.2	12.3	0.9
3	11.2	11.0	7.2	11.2	11.9	11.4	12.0	11.4	1.6	10.9	1.5
4	10.7	11.3	11.0	8.8	11.7	10.9	11.7	11.8	1.8	11.0	1.0
5	11.3	11.7	11.7	11.3	10.4	11.4	11.4	11.6	2.3	11.4	0.5
6	11.2	11.2	11.6	11.2	11.5	8.1	11.8	11.7	1.8	11.0	1.2
7	12.0	12.2	12.5	12.2	12.8	12.2	10.9	12.5	3.1	12.2	0.6
8	10.8	11.6	11.0	11.2	11.9	11.3	11.9	9.4	2.0	11.1	0.8
									2.3	11.3	1.0
									(Average)	(Average)	(Average)

The expected distribution system losses and their expected variances for each of the three source-fiber-detector combinations are presented in Table 4. Note that any of these combinations can provide the required signal power to transmit NRZ data through the system of Figure 17 at a  $10^{-11}$  BER.

A second possible system configuration is shown in Figure 20. This system uses a reflection star coupler as well as access or Tee couplers. It requires half the fiber and half the fiber-to-fiber connectors of the system shown in Figure 17.

Analysis of this system is straightforward. The optimum coupling ratio in the Tee couplers is 3 dB, and the typical excess loss of such a coupler is 1 dB. Consequently, this system requires an additional 7 dB to overcome distribution system loss. Referring again to Table 2 we see that only Case III, using the Hitachi laser, is a viable system. The Bell-Northern LED can be used provided we are willing to accept a reduced system lifetime. If we allow only a 2.8-dB margin for aging of the Bell-Northern source, this system has just enough margin.

#### B. ELECTRICAL POWER CONSUMPTION

In this section, we calculate the expected electrical power consumption for each of the three proposed source-fiber-detector systems. The dominant power-consuming element for each system is found to be the source.

The largest practical load resistor that can be employed in a 10 Mb/sec PIN diode system is about 16 k $\Omega$ . (Larger resistors cause signal power to be diverted from the load resistor by the stray capacitive reactance located in the PIN diode junction.) Such a load resistor is likely to be the parallel impedance of a resistive divider used to bias a transistor. If we assume that FETs are used in the receiver to minimize power consumption, then the power dissipated in the load resistor is dominant. An upper bound estimate of the power consumed in the receiver can be found by calculating the maximum power that can be dissipated in a 16-k $\Omega$  resistor. If the supply voltage is 5 V, the maximum power dissipation in the receiver is about 2 mW.

Table 4. Expected Distribution System Losses for Three Source-Fiber-Detector Combinations. In all cases, an average received optical power of -42 dBm is assumed to be required for satisfactory system operation.

Source	Input Coupling Loss, dB	Connector Loss, dB	Fiber Attenuation, dB	Star Coupler Splitting, dB	Star Coupler Excess, dB	Source Degradation Allowance, dB	Total Distribution System Loss, dB	Expected Variance, dB	Source Power, dBm	Margin, dB
LD IRE-150	8.1	2.8	0.4	15.1	3.3	3.0	32.7	5.5	0.0	3.8
BN 40-3-30-3	1.4 <sup>a</sup>	2.8	1.0	15.1	3.3	3.0	26.6	3.7	-4.9	6.8
Hitachi HLP-2400	3.0	2.8	1.0	15.1	2.3	6.0	30.2	3.8	+1.8	9.8

<sup>a</sup>Due to area mismatch between fiber core and pigtail core only, there will be additional loss if the NAs do not match.

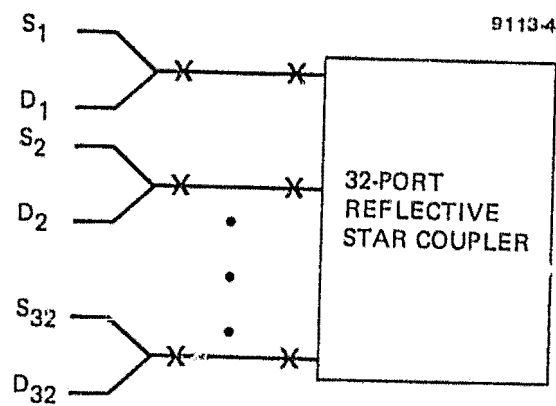


Figure 20. A second system configuration employing a reflection star coupler.

The maximum power consumed by the source can also be estimated. The power consumed by MOS-FET drivers is negligible, typically in the microwatt range. If we assume a 50% duty factor for the data, we can calculate the electrical power consumed by each of the three sources (see Table 5). Table 5 also presents the maximum power consumed by a terminal if it hangs up in the "on" state and the maximum power consumed by the system assuming all 32 sources hang up in the "on" state.

### C. THE EFFECTS OF TEMPERATURE ON BUS PERFORMANCE

Section 5.A discussed the effective power launched into a fiber. Here only the notion that  $P_o$   $\mu$ W of optical power is launched into the fiber is necessary; consequently, the discussion in this section is quite general. The fiber lengths are taken to be short enough that fiber attenuation is negligible. The optical power at the receiver  $R_x$  is given by

$$P_f(T) = \frac{P_o(T)\alpha(T)^2 C^4(T)\epsilon_f(T)}{N}, \quad (30)$$

where  $\epsilon_f$  is the excess loss of the star coupler, and  $\alpha(T)$  is the glass fiber attenuation as a function of temperature  $T$ . The calculations and values used in Section 5.A are typically valid for room temperature ( $\approx 23^\circ\text{C}$ ). If this reference temperature is designated by  $T_o$ , then

Table 5. Power Consumption of Three Typical Sources

Source	Power Consumption, mW		
	50% Duty Factor per Terminal	100% Duty Factor per Terminal	Worst Case If All Terminals Turn On
LD IRE-150	250	500	16,000
BN 40-3-30-3	375	750	24,000
Hitachi HLP-2400	75	150	4,800

6815

the relative bus performance as a function of T can be assessed from the simple ratio  $P_f(T)/P_f(T_0) = R(T)$ :

$$R(T) = \left( \frac{P_o(T)}{P_o(T_0)} \right) \left( \frac{\alpha(T)}{\alpha(T_0)} \right)^2 \left( \frac{C(T)}{C(T_0)} \right)^4 \left( \frac{\epsilon_f(T)}{\epsilon_f(T_0)} \right) . \quad (31)$$

The temperature range of interest is from  $-20^\circ\text{C}$  to  $60^\circ\text{C}$  so that for the launch power ratio we can use the values shown in Figure 21 for an IRE160FB LED as typical of LED performance. The attenuation ratio for a glass-on-glass fiber is given in Figure 22. The induced attenuation coefficient will be considered to be zero from  $+10^\circ\text{C}$  to  $+60^\circ\text{C}$  since that seems to be the trend indicated by Figure 22.

The connector loss  $C(T)$  here refers specifically to a Hughes-built fiber-optic ferrule, No. 1127361, without the connector body assembly. Prior experiments on temperature effects on these ferrules indicated that considerable mechanical stresses could be induced at the glass fiber/brass ferrule interfaces. However, a modification to the fiber ferrule mounting approach permitted greatly reduced stresses with consequent excess attenuation of 0.03 dB at  $-20^\circ\text{C}$  and 0.02 dB at  $+60^\circ\text{C}$ . The implication is that these special ferrules must be requested where temperature shock is expected to be part of the system application.

The remaining factor is the variation of excess loss with temperature. An important distinction must be made here. The fused fiber-optic junction must typically be mounted on some fixture with subsequent mounting in a connector housing. The materials used in the mounting of the fused junction (e.g., epoxy, wax) will have a substantial effect on the temperature behavior of this junction. For present purposes, no mounting of the fused junction will be considered. It is assumed that temperature has no effect on the tapping ratio or excess loss. (No measurements to contradict this assumption have been made.) With these assumptions and data,  $R(60^\circ\text{C})$  becomes:

$$R(60^\circ\text{C}) = \left( \frac{80}{100} \right) (1)^1 (0.99)^4 (1) = 0.77 \text{ or } -1.1 \text{ dB} . \quad (32)$$

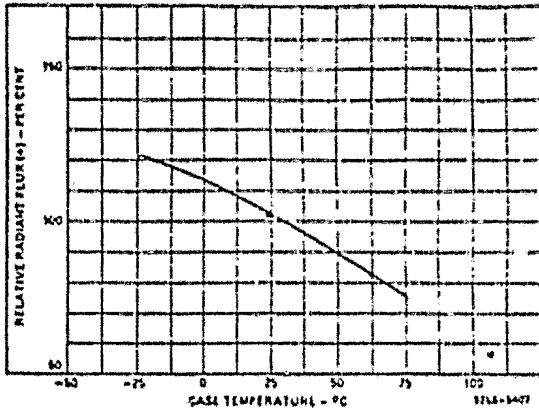
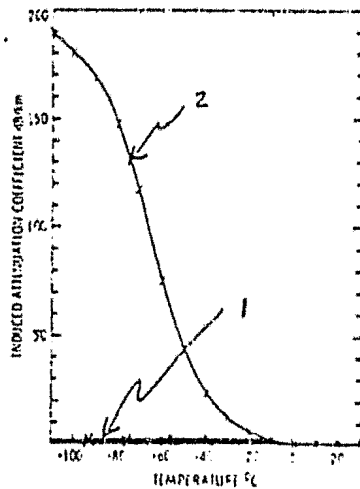


Figure 21. Temperature dependence of the output power of an LED.



- 2 Corning fiber with polyurethane jacket
- 1 Corning fiber without polyurethane jacket

Figure 22. Induced attenuation coefficients as a function of temperature for CVD step-index fiber with polyurethane jacket.

The average signal power required to maintain a given data integrity is:

$$\bar{P}_{sig} = \frac{Q}{2r} \left[ eQ_{FB} + \frac{2}{G} \sigma_o \right] , \quad (33)$$

where

$$\sigma_o = \left[ eI_{DB} G^2_{FB} + eI_{dS} B + \frac{2KT}{R_L} B + I_{na}^2 \right]^{1/2} . \quad (34)$$

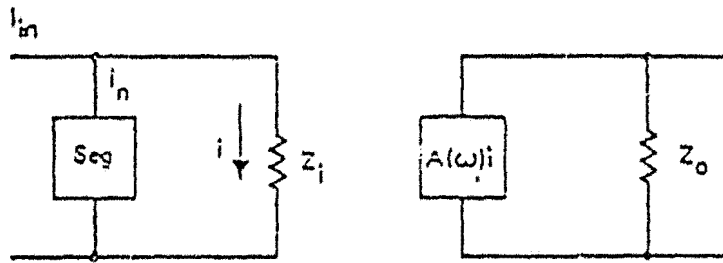
Here a new term  $I_{na}$  has been added.  $I_{na}$  is defined as the equivalent pre-amp input noise current. A brief and simplified discussion of amplifier noise yields an approximate formula for  $I_{na}$ .

Consider the amplifier noise for SiFET and bipolar transistor input stages as shown in Figure 23. The impedance  $Z$  is the parallel combination of the input impedance of the amplifier and the output impedance from the previous stage.  $A(\omega)$  is the current amplification of the stage, and  $S_{eq}$  is the frequency-dependent equivalent noise current spectral density of a noise generator that gives the same output noise spectral density as internal noise sources. The equivalent noise current spectral density is

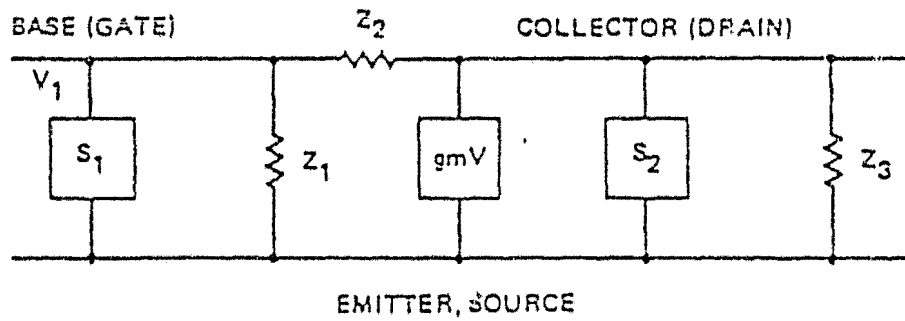
$$S_{eq} = S_{eq_1} + S_{eq_2} , \quad (35)$$

where the first term is the contribution of the input, and the second is the contribution of the output noise current spectral densities. Then

$$S_{eq}(\omega) = S_1 + S_2 \frac{\omega^2 C_T^2 + (R_{IN})^{-2}}{g_m^2} , \quad (36)$$



(a) General equivalent noise circuit



(b) Specific model for FET and bipolar transistors

Figure 23. Amplifier noise model.

where  $S_2$  has been transformed to an equivalent input current source.  $C_T$  is the sum of detector and amplifier input capacitances. The mean-squared noise current is

$$\overline{i_n^2} = \frac{1}{2\pi} \int_0^\omega S_{eq}(\omega) d\omega \quad (37)$$

For a SIFET,

$$S_1 = \frac{4kT\theta(\omega C_T)^2}{g_m} + 2e i_g \quad (38)$$

and

$$S_2 = 4kT\Gamma g_m \quad (39)$$

where  $\theta$  is 1/10 to 4/15, depending on the FET, and  $\Gamma$  is 2/3. The gate current  $i_g$  is generally quite small, and  $R_{IN}$  can be made quite large. Thus,

$$S_{eq} \approx \frac{2.8kT(\omega C_T)^2}{g_m} \quad (40)$$

To minimize the noise,  $g_m/C_T^2$  should be maximized. The mean-squared noise current in the bandwidth  $B$  for a SIFET  $i_{nFET}^2$  is:

$$\overline{i_{nFET}^2} = \frac{2.8kT}{6\pi g_m} C_T^2 \omega_{max}^3 = \frac{kT(2\pi C_T)^2 B^3}{g_m} \quad (41)$$

or

$$\sqrt{\overline{i_{nFET}^2}} = \sqrt{\frac{kT(2\pi C_T)^2}{g_m}} B^{3/2} \quad (42)$$

Using typical values of  $C_T = 10$  pF and  $g_m = 0.006$  mho, the rms noise current is

$$\sqrt{i_{nFET}^2} \approx 5 \times 10^{-20} B^{3/2} \quad , \quad (43)$$

which is about 1.6 nA for  $B = 10$  MHz.

For a bipolar transistor,  $R_{IN}$  may be adjusted by varying the input bias current  $i_B$ :

$$R_{IN} \approx \frac{kT}{e i_B} \quad . \quad (44)$$

Then it follows that

$$S_1 = 2 e i_B \approx \frac{2kT}{R_{IN}} \quad . \quad (45)$$

The transconductance  $g_m$  can be approximated by  $\beta/R_{IN}$ , where  $\beta$  is the current gain. Substituting this approximation into the expression for  $S_2$  yields

$$S_2 = 2e i_C = 2e\beta i_B = \frac{2kT}{R_{IN}} \beta \quad , \quad (46)$$

where  $i_C$  is the collector current. This yields

$$s_{eq} = \frac{2kT}{R_{IN}} + 2kTR_{IN} \left( \frac{\omega^2 C_T^2 + 1/R_{IN}^2}{\beta} \right) \quad . \quad (47)$$

The rms noise current in the bandwidth  $B$  can be evaluated and minimized by varying  $R_{IN}$ . The optimal value of  $R_{IN}$  is  $\sqrt{3/2} \sqrt{C_T B}$ . To accommodate the system bandwidth, the low-pass filter network consisting of  $R_{IN}$  and  $C_T$  should be such that

$$R_{IN} C_T \leq (2\pi B)^{-1} \quad . \quad (48)$$

Acknowledging this but continuing to calculate the minimum noise, one obtains

$$\sqrt{\overline{i_n^2}}_{\text{BIPOLAR}} = \sqrt{\frac{4kT}{3\beta} \frac{2\pi C_T}{B}} \quad (49)$$

For  $C_T = 10$  pF and  $\beta = 160$ , the rms noise current is

$$\langle \overline{i_n^2} \rangle_{\text{BIPOLAR}}^{1/2} = 2 \times 10^{-16} B \quad (50)$$

which is about 2 nA for 10 MHz. If  $R_{IN}$  is evaluated at  $1/2 C_T B$ , then the rms noise current is increased to about  $7 \times 10^{-16} B$ . Since the bipolar front-end noise and FET front-end noise are proportional to  $B$  and  $B^{3/2}$ , respectively, at high frequencies (above 14 MHz), the bipolar front-end shows superior noise performance. Using the lower value for a SiFET preamp of 1.6 nA at 10 MHz, the required average power  $\overline{P}_{\text{sig}}$  can be calculated for the two extreme temperatures (i.e.,  $-20^\circ\text{C}$  and  $+60^\circ\text{C}$ ). With  $i_{na} = 1.6$  nA at  $T = -20^\circ\text{C} = 253^\circ\text{K}$ , we see that

$$\begin{aligned} \sqrt{\overline{i_n^2}}_{\text{BIPOLAR}} &= \left(\frac{T}{T_0}\right)^{1/2} i_{na}(T_0) \\ &= \left(\frac{253}{300}\right)^{1/2} (1.6 \text{ nA}) \text{ at } 10 \text{ MHz} \\ &= 1.46 \text{ nA at } 10 \text{ MHz} \quad (51) \end{aligned}$$

where the assumption is made that the transconductance of the FET is fairly insensitive to  $T$  in the  $-20^\circ\text{C}$  to  $+60^\circ\text{C}$  range. Therefore, the required  $\sigma_0$  for an HP 5082-4205 pin detector is

$$\begin{aligned}
i_{ns}(-20^\circ\text{C}) &= \left( eI_{DB}^2 B^2 + eI_{DB} B + \frac{4kT}{R_L} B + i_{na}^2 \right)^{1/2} \\
&= \left( 10^7 (1.6 \times 10^{-19} \text{C}) (0.05 \times 10^{-10} \text{A}) + \frac{4(1.38 \times 10^{-23} \text{J/K})(253^\circ\text{K})}{1.6 \times 10^4 \Omega} 10^7 \right. \\
&\quad \left. + (1.46 \times 10^{-9})^2 \right)^{1/2} \\
&= 3.29 \times 10^{-9} \text{ A} .
\end{aligned} \tag{52}$$

The required incident average optical power  $\bar{P}_{sig}$  with  $Q = 7$  and  $r(-20^\circ\text{C}) = 0.35 \text{ } \mu\text{A/nW}$  is

$$\begin{aligned}
\bar{P}_{sig}(-20^\circ\text{C}) &= \frac{7}{2(0.35)} \left[ (1.6 \times 10^{-19})(7)10^7 + 2(3.29 \times 10^{-9}) \right] \\
&= 6.6 \times 10^{-8} \text{ W} = -42 \text{ dBm at } 10 \text{ MHz} .
\end{aligned} \tag{53}$$

A similar procedure is used to determine  $\bar{P}_{sig}(+60^\circ\text{C})$ . For  $T = +60^\circ\text{C}$  given with  $I_{ns} = 3.5 \text{ } \mu\text{A}$ , we have

$$\begin{aligned}
\bar{P}_{sig}(+60^\circ\text{C}) &= \frac{7}{2(0.55)} \left[ (1.6 \times 10^{-19})(7)10^7 + 2(4.13 \times 10^{-9}) \right] \\
&= 5.26 \times 10^{-8} \text{ W} = -42.7 \text{ dBm} .
\end{aligned}$$

At first glance it might seem that  $-42.0 \text{ dBm}$  is high in terms of required optical power, but one must recall that a BER of  $10^{-11}$  is required and that the equivalent amplifier input noise current was included.

Taking the values for system 2, which employs the Bell Northern LED source,  $-4.9 \text{ dBm}$  into the fiber results in  $P_f(300^\circ\text{K}) = -32 \text{ dBm}$  incident on the detector. From Eq. 31, the relative bus performance at  $60^\circ\text{C}$  is found to be:

$$\begin{aligned}
\bar{P}(60^\circ\text{C}) &= (0.76)(0.66 \text{ } \mu\text{W}) = 0.50 \text{ } \mu\text{W} \\
&= -33 \text{ dBm}
\end{aligned} \tag{55}$$

and similarly for  $T = -20^{\circ}\text{C}$

$$\begin{aligned}\bar{P}(-20^{\circ}\text{C}) &= (1.15)(0.66 \mu\text{W}) = 0.76 \mu\text{W} \\ &= -31 \text{ dBm} \quad . \quad (56)\end{aligned}$$

This means that, in the given temperature range of  $-20^{\circ}\text{C}$  to  $+60^{\circ}\text{C}$ , the incident optical power on the detector should vary by approximately  $\pm 1$  dBm and both  $\bar{P}(60^{\circ}\text{C})$  and  $\bar{P}_o(-20^{\circ}\text{C})$  are well above the required  $-42$  dBm calculated for  $\bar{P}_{\text{sig}}$  with  $\text{BER} = 10^{-11}$ .

A last remaining item of interest is how the detector noise (i.e., the NEP) varies over this temperature range. If one designates the NEP at room temperature as  $\text{NEP}(T_o)$ , then using an approximate relation<sup>4</sup> gives us the NEP(T) at some other temperature,

$$\text{NEP}(T) = \left(\frac{T}{T_o}\right)^{5/2} \text{NEP}(T_o) \quad , \quad (57)$$

so that with  $\text{NEP}(T_o) = 44 \times 10^{-12}$  W previously calculated, we see that

$$\begin{aligned}\text{NEP}(+60^{\circ}\text{C}) &= \left(\frac{353}{300}\right)^{5/2} (44 \times 10^{-12} \text{ W}) \\ &= 6.6 \times 10^{-11} \text{ W} = -72 \text{ dBm} \quad (58)\end{aligned}$$

and

$$\begin{aligned}\text{NEP}(-20^{\circ}\text{C}) &= \left(\frac{253}{300}\right)^{5/2} (44 \times 10^{-12} \text{ W}) \\ &= 2.87 \times 10^{-11} \text{ W} = -75 \text{ dBm} \quad . \quad (59)\end{aligned}$$

The conclusion to be drawn is that, for this bus structure over this temperature range, no degradation of consequence should be anticipated.

#### D. CONCLUSIONS

The analysis of the last section indicates that temperature will play a very minor role in the design of fiber-optic data buses for spacecraft. Over the temperature range of  $-20^{\circ}\text{C}$  to  $+60^{\circ}\text{C}$ , we expect no more than 2-dB variation in the received signal-to-noise ratio.

The analysis of Section 5.A can be used to determine the source power required in a typical bus application. Consider again the basic 32-port transmission star system of Figure 17. The source power required to maintain a  $10^{-11}$  BER at a 10 Mbit/sec data rate for this system can be determined. First, assume that the source is an LED and that the detector is optimized and requires  $-42$  dBm of optical power to operate at a  $10^{-11}$  BER. Next, assume that the excess loss of the star coupler is 3.0 dB independent of the number of ports in the coupler. Finally, assume that the cross-sectional area of the source exactly matches the area of the fiber core and that the fiber is plastic-clad silica with a 0.35 NA. Then the input coupling loss is 8.1 dB. If low-loss fiber is used, the distribution system loss is negligible for a spacecraft bus. Connector loss is 2.8 dB, and 3.0 dB of margin is provided to account for lifetime variations of the source. An additional 6.8 dB of margin is included to account for variations in input coupling, splitting in the star coupler, variations in insertion loss of connectors, etc. This is a total of 23.7 dB. There is an additional attenuation of  $10 \log M$  caused by the splitting factor in the star coupler. Consequently, the required source power  $S$  is

$$S = -42.0 + 23.7 + 10 \log M \text{ (dBm)} \quad . \quad (60)$$

for the transmission star coupler. If a reflection star coupler is used, access couplers will be required; however, two connectors can be removed. The required source power  $S'$  in this case can be calculated from

$$S' = S + 8 \text{ (dBm)} \quad , \quad (61)$$

where the extra 8 dB of attenuation accounts for the tap ratios and excess loss in the access couplers.

The electrical power consumption of the three systems considered in Section 5.A can also be estimated. Eq. 60 describes the optical source power required to achieve a  $10^{-11}$  BER as a function of the number of terminals. Eq. 60 and the functional dependence of optical power output on the drive current for each of the three sources of Section 5.A are combined to determine the required source drive current. The average electrical power consumed is found from the drive current assuming a 50% duty factor and a 5-V power supply. The result of this calculation is presented in Figure 24.

The results of this analysis indicate that a transmission-star fiber-optic data bus serving 32 terminals is feasible. The system can operate over the temperature range expected in a spacecraft application. It is possible to implement such a system using an LED source and PIN diode detector with ample optical power margin. This LED-PIN based system is expected to consume less than 1/8 W of average electrical power per active transmitter-receiver pair.

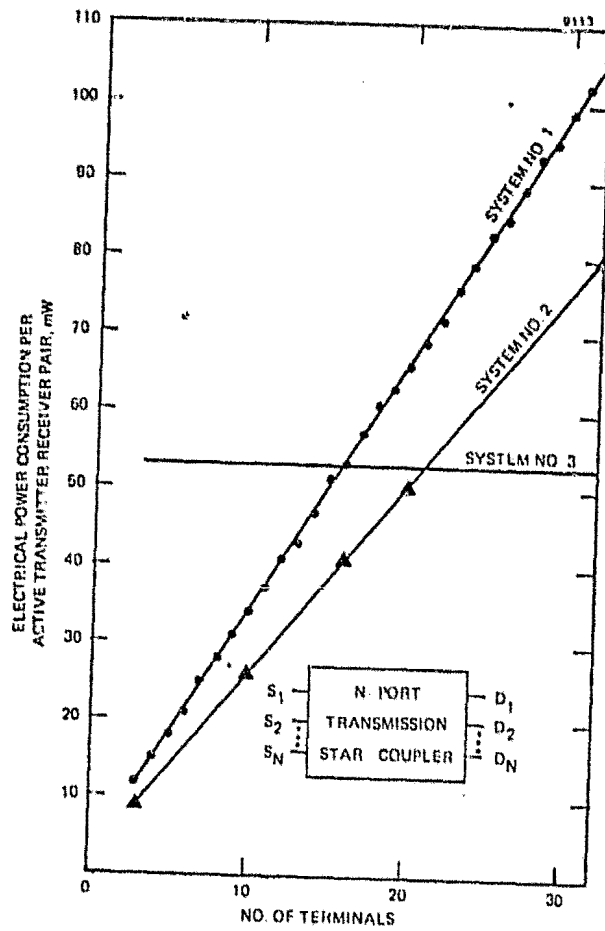


Figure 24. The expected electrical power consumption of a spacecraft data bus as a function of the number of terminals. The systems are those described in Section 5.A.

#### REFERENCES

1. M.A. Holeman, "A Detachable Connector for Multimode Graded Index Optical Waveguides," Deutsch Technical Reprint No. 136, Copyright 1979.
2. G.L. Tangonan et al., "Planar Coupler Devices for Multimode Fiber Optics," presented at Optical Fiber Communications Conference, Washington, D.C., March 6-8, 1978 (unpublished).
3. E.G. Rawson, "Optical Fibers for Local Computer Networks," presented at Optical Fiber Communications Conference, Washington, D.C., March 6-8, 1978 (unpublished).
4. E.H. Putleys, "Modern Infrared Detectors," *Physics in Technology* 4, 202-222, December 1973.
5. W.F. Young and A.R. Johnston, *Appl. Opt.* 17, 3703 (1978).

APPENDIX I

BIBLIOGRAPHY

During this contract, many references pertaining to the contract were located. Those references are presented in this appendix.

D.E. Altman, "Eight Terminal, Bidirectional, Fiber Optic Trunk Data Bus Final Report, July 1974 - June 1975," NELC, San Diego, CA.

D.E. Altman and H.F. Taylor, "Eight-Terminal Bidirectional Fiber Optic Data Bus Employing T-Couplers," Digest of Technical Papers of Conference on Lasers and Electro-Optical Systems, 25-27 May 1976, San Diego, CA.

D.E. Altman, Fiber and Integrated Optics 1, 135 (1977).

J.D. Anderson and E.J. Miskovic, "Fiber Optic Data Bus," 10th Annual Connector Symposium Proceedings 225-42, 1977, Cherry Hill, New Jersey.

G. Arnold and P. Russer, "Modulation Behavior of Semiconductor Injection Lasers," Appl. Phys., Springer Verlag 14, 255 (1977).

M. Barnoski, "Data Distribution Using Fiber Optics," Appl. Opt. 14, 2571 (1975).

M.K. Barnoski, M.D. Rourke, S.M. Jensen, and H.R. Friederich, "Components for Single Strand Fiber Systems," Proceedings EASCON 1976.

A.B. Boullie, Frequenz 32, 91 (1978).

E.J. Friebele, M.E. Gingerich, and G.H. Sigel, "Effect of Ionizing Radiation on Optical Attenuation in Open Silica and Plastic Fiber-Optic Waveguides," Appl. Phys. Lett. 32, 619 (1978).

R.A. Greenwell and G.M. Holma, "A-7 Aloft Economic Analysis and EMI-EMP Test Results," Proceedings AGARD Conference on Optical Fibres Integrated Optics and Their Military Applications, ed. H. Hodara CP 219, London, May 1977.

D.C. Hanson, "Circuit and System Considerations for Integrated Industrial Fiber Optic Data Links," Proceedings Conference on Laser and Electro-Optical Systems, 18, 7-9 February 1978, San Diego, CA.

T.A. Hawkes and J.C. Reymond, "Optical Communications Systems for Aircraft," Proceedings 2nd European Conference on Optical Fiber Communications, Paris, France, September 1976.

A.R. Johnston, "NASA Fiber Optics Tasks," Proceedings Intelcom 77, Atlanta, GA, October 1977.

A.F. Judy and T.D. Mathis, "Welded Optical Fiber Signal Splitter," Technical Digest Optical Fiber Communication Conference, Optical Society of AM, Washington, D.C., March 1979.

B.S. Kawasaki and K.D. Hill, "Low Loss Access Coupler for Multimode Optical Fiber Distribution Networks," Appl. Opt. 16, 1794 (1977).

P.J. Miki et al., Trans. Inst. Electron. and Commun. Eng. Japan Sect. E E61, 229 (1978).

F.L. Pensworth, "Review of Different Approaches to the Standard Interface Problem," proceedings of the National Aerospace Electronics Conference (NAELON), Dayton, OH, May 1973.

D.R. Porter and I.R. Reese, "A Hybrid Configured Fiber Optic Data Bus System," Proceedings 2nd European Conference on Optical Fiber Communications, Paris, France, September 1976.

R.B. Quaimby, "Data Highway Devices and Systems," Optics and Laser Technol. Electro-Optical Systems Design, Electro-Optics/Laser International '76 UK, 9-11 March 1976, Brighton, Sussex, England.

E.G. Rawson, IEEE Trans Commun. COM-26, 983 (1978).

S. Share, R.M. McCracken, and I. Aggarwal, "The Effect of Temperature on the Response of Glass-Clad Optical Waveguides in Ionizing Radiation," IEEE Trans NS21, 1288, 1978.

M.C. Shoquist, "An Advanced Fiber-Optic Processor Interconnect System," 14th IEEE Computer Society International Conference Proceedings, 23 Feb. - 3 Mar. 1977, San Francisco, CA., pp. 248-252.

G.L. Tansonan, O.G. Ramer, L.E. Gorre, H.R. Friedrich, C.K. Asawa, M.K. Barnoski, and D.L. Persechini, "Planar Coupler Devices for Multimode Fiber Optics," Technical Digest, Optical Fiber Communication Conference, Opt. Soc. Am., Washington, D.C., March 1979.

F.W. Thiel, Alta Frequenza 45, 144 (1976).

Y. Ueno and N. Odgi, "Data Highway Using Optical Fiber Cable," Digest of Technical Papers of Conference on Lasers and Electro-Optical Systems, 25-27 May 1976, San Diego, CA.

W.F. Yeung and A.R. Johnston, "Effect of Temperature on Optical Fiber Transmission," Appl. Opt. 17, 3703 (1978).

M.K. Zamen, D.J. Oda, and G.H. Fortescue, "Developmental CP-901 Airborne Digital Computer Fiber Optic Interface for Potential Application in P-3C Aircraft," Proc. of the Tech. Program Electro-Optical Systems Design Conference and International Laser Exposition, Anaheim CA. Nov.11-13,1975.

## BUS RECEIVER TEST RESULTS

This a preliminary report documenting performance characteristics of a demonstration fiber optic data bus system developed by Hughes for JPL. The major system components, shown in Figure 1, are: (1) the transmitter, (2) the star coupler, and (3) the receiver. The measured average optical power levels at critical bus locations are also shown in this figure. The characteristics of each component are described below.

Transmitter. The transmitter includes an LED driver circuit, and a pigtailed LED. The pigtail is terminated in a Hughes connector. The LED is type IRF160FB from Laser Diode Laboratories.

The transmitter requires  $\pm 5V$  power supply. When the LED is driven with a 100 mA, 50% duty cycle pulses, the average optical power level at the connector is -11 dbm. It drops by 10 db when the drive current drops to 34 mA. At 30 mA, the optical power drops to -27 dbm. The graph of the drive current vs the optical power output is shown in Figure 2.

Star Coupler. The 8 port fused star coupler includes 50 meters of step index fiber in each of two opposite legs. The fiber contains a splice and is terminated in Hughes connector contacts. The average optical power coupled into the star is -13 dbm. The power at the output is -27 dbm. The 14 db loss includes: (1) 9 db power division loss in the star, (2) 2 db connector loss, and (3) fiber, splice and excess star losses.

A short graded index fiber terminated at both ends in Hughes connector contacts is included between the star output and the receiver input. The loss through this fiber "jumper" is 6 db, of which about 3 db is due to the modal mismatch between step and graded index fibers. The "jumper" is provided to simulate the losses due to additional in-line connectors which may be required for some applications.

Receiver. The receiver includes a pigtailed H.P. 4220 PIN diode and amplifier circuits. The pigtail is terminated in a Hughes connector. The average optical power level at the face of the diode is calculated to be -35 dbm. The receiver requires +6V - 5V power supply and 230 mA of current.

The receiver block diagram is shown in Figure 3. The transresistance pre-amplifier is of a cascade configuration. The post-amplifier differentiates the incoming signal and further amplifies it. The digital circuitry decodes the differentiated signal and provides TTL outputs. The  $C^+$  comparator sets the latch on the positive going pulse, while the  $C^-$  comparator re-sets it on a following negative going pulse. The magnitude of each pulse has to be at least 10 mV.

Figure 4 shows the operation of the receiver at 10 MHz and at 1 MHz. The upper trace is the random NRZ data input to the transmitter and lower trace is the output (delayed in time) of the receiver. The corresponding signal levels at the outputs of the pre-amplifier and the post-amplifier are shown in Figure 5. The top figure illustrates the good high frequency response to support 10 MBPS operation. However, Figure 5b shows that the selected bandwidth does not fully differentiate the signal. Since JPL requested operation from 1 to 10 MHz, this was compromised in order to achieve the excellent response at 1 MHz shown in Figure 5c.

The response of the post-amplifier to a short burst of pulses at 10 MHz and at 1 MHz is shown in Figure 6. Note that the transient response at 10 MHz is such that the  $C^-$  comparator would have to be set very close to zero in order to catch the first bit. However, normally a  $1\frac{1}{2}$  to 2 bit sync pulse would be used, and under those conditions, no bits should be missed.

Figure 7 shows the measured bit error rate vs average optical power at the receiver. Random 10 MBPS NRZ data was used at the input to the transmitter. The measurements show receiver sensitivity of -39 dbm for error rate less than one in  $10^9$  bits. Under those conditions, the receiver dynamic range is 16 db.

## Bus Receiver Test Results

Page 3  
94-51T/136

A new pre-amplifier design, currently under final stages of development at Hughes, appears to offer even better performance. Preliminary measurements show at least 3 db improvement in receiver sensitivity and 7 db more dynamic range. Electrical power consumption should also be lower in the new design.

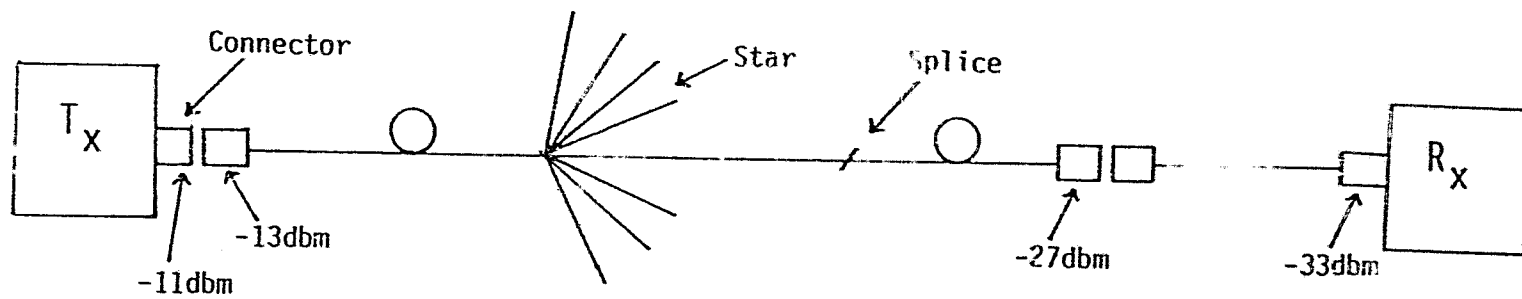


FIGURE 1. BUS RECEIVER SYSTEM

ORIGINAL PAGE IS  
OF POOR QUALITY

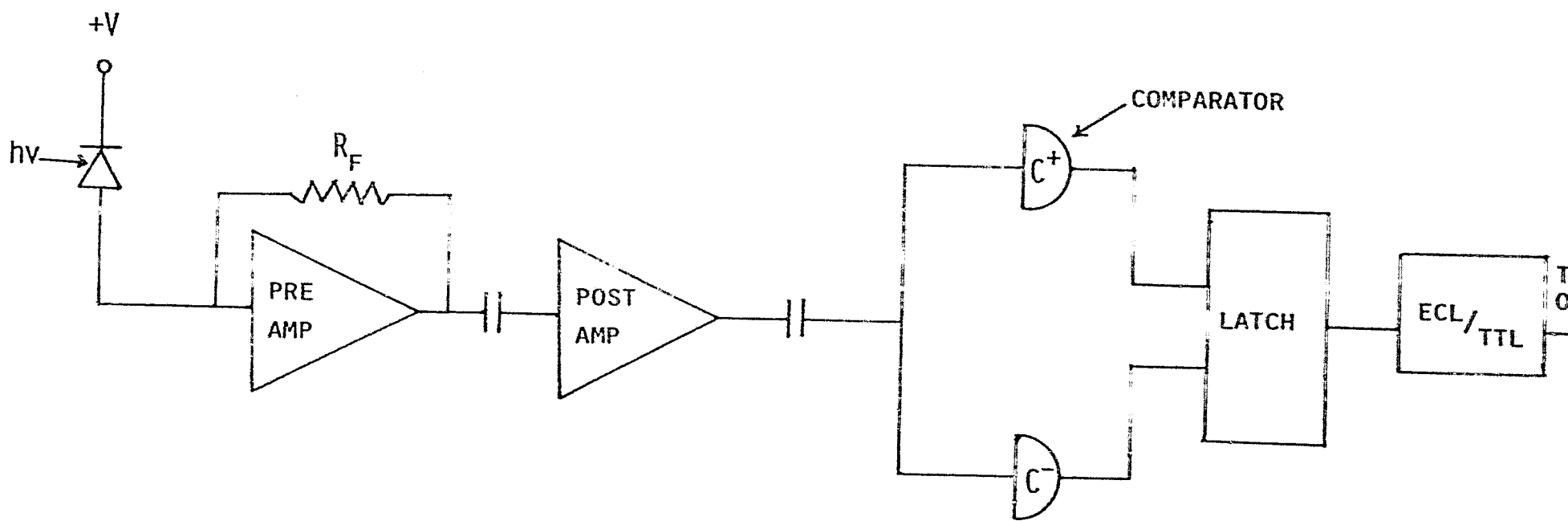
Page 5  
94-517, 136

Figure 2 LED DRIVE CURRENT  
VS  
OPTICAL POWER OUTPUT

Average Optical Power Out ( $\mu\text{W}$ )

100

10



74

FIGURE 3. RECEIVER BLOCK DIAGRAM

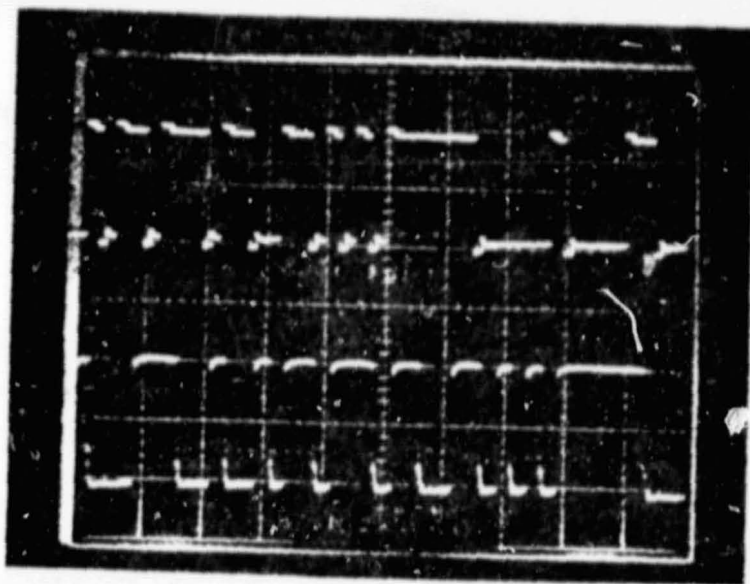


Figure 4(a) Receiver output at 20 MHz

ORIGINAL PAGE IS  
OF POOR QUALITY

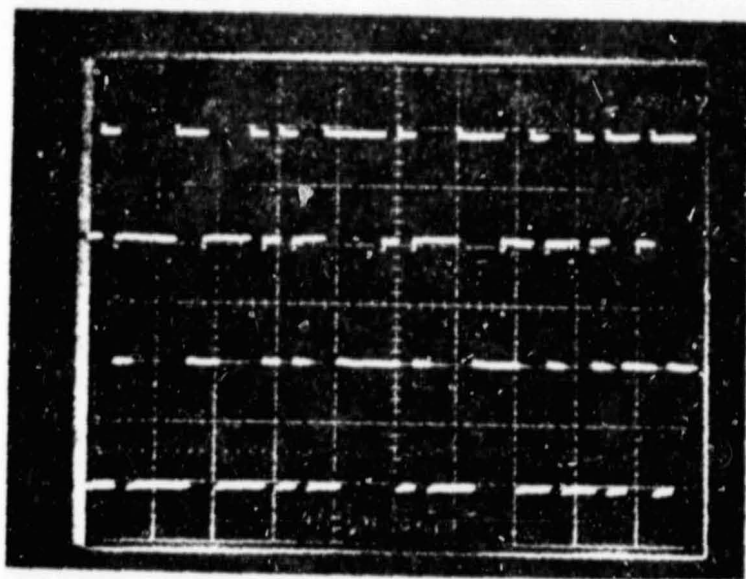


Figure 4(b) Receiver output at 1 MHz

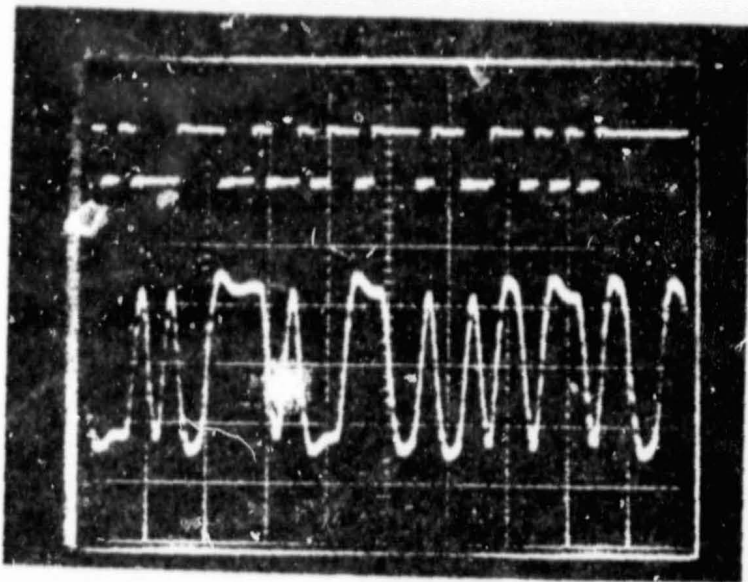


Figure 5(a)  
Pre Amp Output at 10 MHz

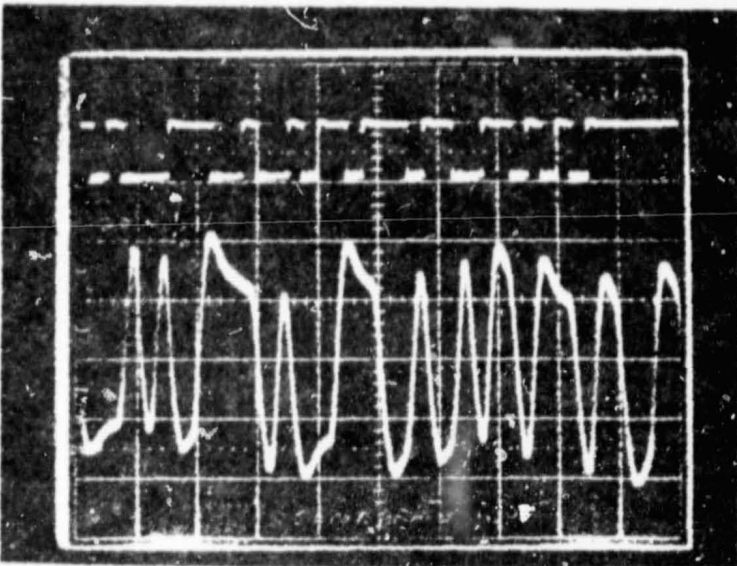


Figure 5(b)  
Post Amp Output at 10 MHz

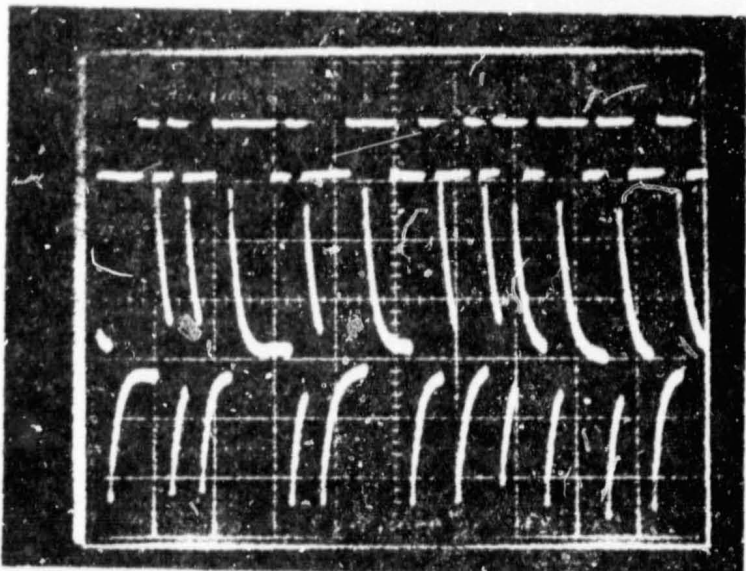


Figure 5(c)  
Post Amp Output at 1 MHz

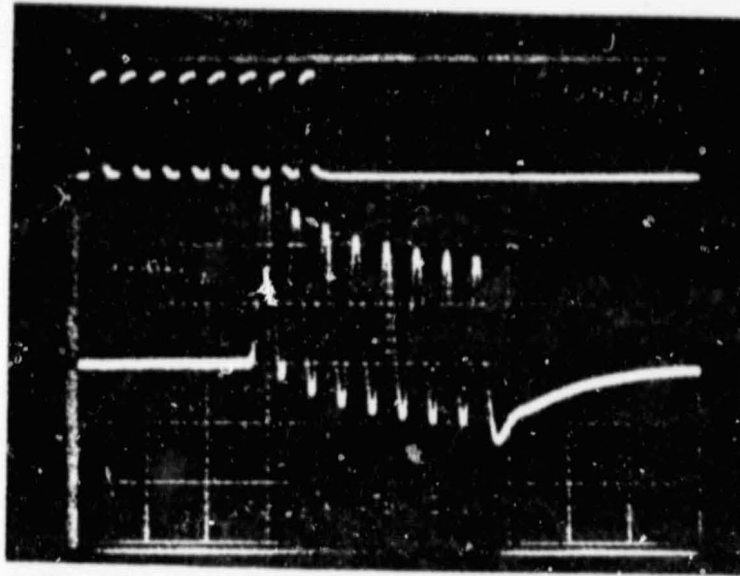


Figure 6(a) Transient Response at 10 MHz

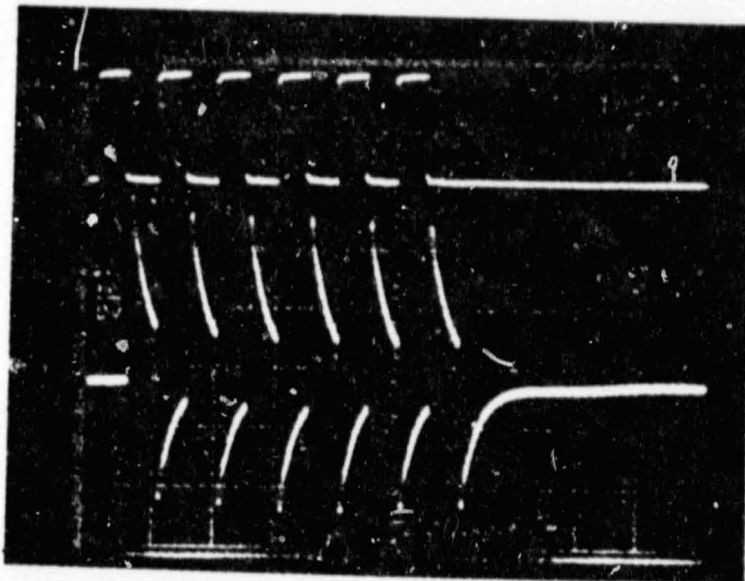
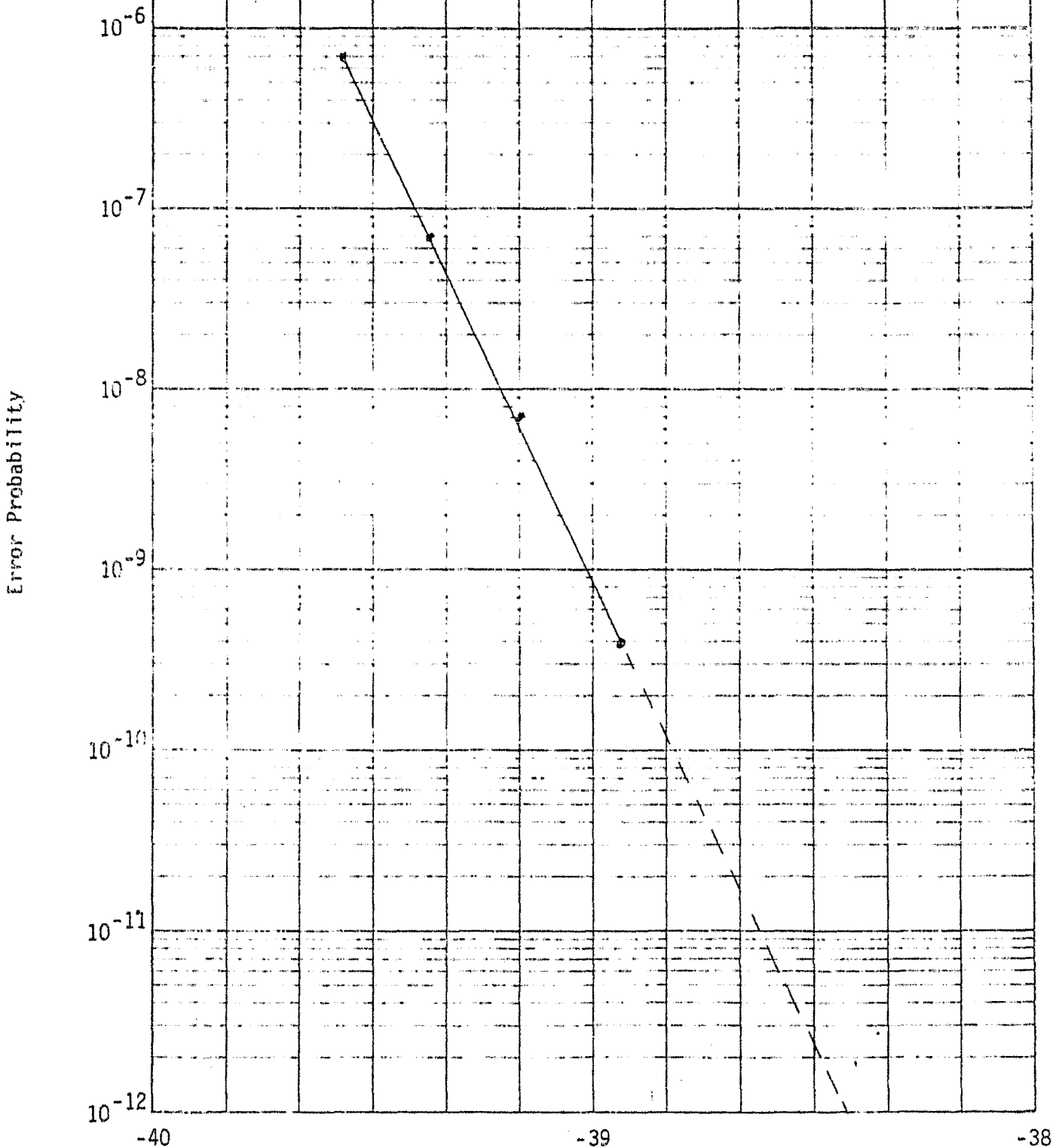


Figure 6(b) Transient Responses at 1 MHz

ORIGINAL PAGE IS  
OF POOR QUALITY

Figure 7. ERROR PROBABILITY VS AVERAGE OPTICAL SIGNAL POWER



Average Optical Signal Power in dbm

OF POOR QUALITY